

1 **The impact of individual land surface properties on terrestrial climate and**
2 **atmospheric feedbacks**

3 Marysa M. Laguë*

4 *University of Washington Department of Atmospheric Sciences, Seattle, WA, USA*

5 Gordon B. Bonan

6 *National Center for Atmospheric Research, Boulder, CO, USA*

7 Abigail L. S. Swann

8 *University of Washington Department of Atmospheric Sciences and Department of Biology,*
9 *Seattle, WA, USA*

10 **This article is a non-reviewed preprint published at EarthArXiv**

11 **Notice:**

From the AMS Copyright Policy section 7: This work has not yet been peer-reviewed and is provided by the contributing author(s) as a means to ensure timely dissemination of scholarly and technical work on a noncommercial basis. Copyright and all rights therein are maintained by the author(s) or by other copyright owners. It is understood that all persons copying this information will adhere to the terms and constraints invoked by each author's copyright. This work may not be reposted without explicit permission of the copyright owner. This work has been submitted to the *Journal of Climate*. Copyright in this work may be transferred without further notice.

17

18

19 <https://www.ametsoc.org/index.cfm/ams/publications/ethical-guidelines-and-ams-policies/ams->
20 [copyright-policy/](https://www.ametsoc.org/index.cfm/ams/publications/ethical-guidelines-and-ams-policies/ams-copyright-policy/)

21 **Corresponding author address:* Marysa M. Laguë, University of Washington Department of Atm-
22 spheric Sciences, Box 351640, Seattle WA, 98195, USA

23 E-mail: mlague@uw.edu

ABSTRACT

24 While the land surface is highly dependent on the atmosphere above it,
25 changes in the land surface can drive large responses in the atmosphere on
26 local, regional, and global scales. Surface properties control the partitioning
27 of energy within the surface energy budget. Changes in surface energy fluxes
28 can impact the atmosphere on local scales through changes in temperature or
29 cloud cover, and global scales through changes in large scale atmospheric cir-
30 culation. We test the sensitivity of the atmosphere to global changes in three
31 land surface properties: albedo, evaporative resistance, and surface roughness.
32 We show that the climate impact of changing a land surface property differs
33 drastically between simulations run with an offline land model alone com-
34 pared to coupled land-atmosphere simulations which allow for atmospheric
35 feedbacks. Atmospheric feedbacks play a critical role in defining the temper-
36 ature response to changes in albedo and evaporative resistance, particularly in
37 the extra-tropics, with atmospheric feedbacks accounting for over 50% of the
38 surface temperature response to changing albedo in over 80% of land areas.
39 Changes in each surface property drive spatially distinct patterns of atmo-
40 spheric feedback-driven surface temperature changes. By individually testing
41 the climate impact of the different surface properties associated with vegeta-
42 tion change, we improve our fundamental understanding of both how and why
43 changes in vegetation cover drive responses in the atmosphere. Additionally,
44 we develop understanding of the role of individual land surface properties in
45 controlling climate across spatial scales – critical to understanding the effects
46 of land-use change on Earth’s climate.

47 **1. Introduction**

48 While the impact of climate on plants has long been appreciated, the impact of plants on climate
49 is an emerging area of research. The effects on climate of changing vegetation vary depending
50 on the location of the vegetation change. Tropical deforestation can lead to warming, because of
51 the high rate of evaporative cooling driven by transpiration (Bonan 2008b). Increasing tree cover
52 in the mid-latitudes has been shown to modify local climate and cloud cover, as well as drive
53 shifts large-scale circulation by modifying global energy gradients (Swann et al. 2012; Laguë
54 and Swann 2016). Changes in vegetation at high latitudes can modify surface temperatures both
55 through surface albedo and the atmospheric water vapor changes (Bonan 2008b; Swann et al.
56 2010). The effects of historical land-use and land cover change have been shown to impact surface
57 temperatures in offline (land-only models), while future land use has been proposed as a potential
58 method of mitigating anthropogenic climate change (Canadell and Raupach 2008). In addition to
59 directly influencing surface climate, interactions between vegetation change and the atmosphere
60 can drive atmospheric feedbacks and teleconnections which further influence surface climate, both
61 locally and remotely (Bonan 2008b; Swann et al. 2012; Laguë and Swann 2016; Kooperman et al.
62 2018).

63 Much of our understanding of vegetation-climate feedbacks comes from models of Earths' land-
64 atmosphere-ocean-sea ice system. Land surface models represent the biogeophysical coupling
65 between the land and atmosphere through fluxes of momentum, energy, and water, which are in
66 turn controlled by the land surface albedo, rates of evapotranspiration, and surface roughness. The
67 climate at the land surface is determined both by the background regional climate as well as the
68 characteristics of the local land surface; changes in individual land surface properties each have a
69 different impact on surface climate. Albedo directly controls the amount of solar energy absorbed

70 by the surface; aerodynamic roughness controls the efficiency of turbulent energy exchange with
71 the atmosphere; and the resistance to evaporation controls how much water can move from the
72 land surface to the atmosphere. Changes in vegetation modify each of these surface properties
73 in different ways. For example, consider a forest and a grassland. The forest is very tall, and
74 thus aerodynamically rough compared to the grassland; this facilitates more efficient turbulent
75 exchange of energy with the atmosphere. Forests are much darker than grasslands - they have a
76 lower albedo, and thus absorb a larger fraction of incident solar radiation than grasslands. Some
77 vegetation has roots which can access water deep in the soil even when surface soils are dry, allow-
78 ing for water to flux from the land to the atmosphere in dry atmospheric conditions. Additionally,
79 the leaf area and stomatal resistance of different types of vegetation control how difficult it is for
80 water to pass through vegetation into the atmosphere. Shifting the land cover from one type of
81 vegetation to another changes many these surface properties, and changes in different properties
82 of the land surface drive changes in the surface energy budget and surface temperatures. Through
83 these changes in energy fluxes, the land can drive changes in the atmosphere, ranging from small
84 local changes in air temperatures or cloud cover to large, global-scale changes in circulation.

85 Surface energy fluxes are the complex outcome of biogeophysical processes at the land surface,
86 with changes in any individual surface property having a different effect on climate. In modern
87 Earth System Models, it is often difficult to individually perturb a single land surface property.
88 In a model such as the Community Land Model (CLM, (Lawrence et al. 2018)), surface albedo
89 is the complex result of leaf and stem reflectance and transmittance, the orientation of leaves, the
90 amount of leaf and stem material, interception of snow in the canopy, soil color, soil moisture, and
91 snow cover. Evaporation is calculated from stomatal conductance for transpiration, a conductance
92 for soil evaporation, and evaporation of intercepted water held externally on foliage. Stomatal
93 conductance itself depends on photosynthetic rates as determined by the photosynthetic capacity

94 of the canopy as modified by light absorption, temperature, vapor pressure deficit, soil moisture
95 availability, and atmospheric CO₂ concentration. Because of these complex relationships, many
96 seemingly simple properties of a land surface model, such as albedo, are actual emergent prop-
97 erties of the model. As such, it is difficult to directly prescribe a change in a specific surface
98 property such as albedo or evaporative resistance, or anticipate how a change in vegetation type
99 may actually influence these surface properties. Davin et al. (2010) isolated the individual effects
100 of albedo, evaporative resistance, and surface roughness when comparing the climate effects of
101 forests versus grasslands using the ORCHIDEE land model, but such a modeling protocol is un-
102 common. Alternatively, one can try to diagnose the relative contribution of each term to surface
103 temperature from model results or observations (Lee et al. 2011; Boisier et al. 2012).

104 Modifying surface energy fluxes through vegetation change has a direct impact on surface cli-
105 mate. However, the changes in the atmosphere in response to these initial surface flux changes can
106 feed back on surface climate, both locally and remotely. For example, modifying forest cover in
107 the mid-latitudes can alter mid-latitude cloud cover, which in turn modifies the amount of sunlight
108 reaching the land surface (Laguë and Swann 2016). Vegetation can also modify local precipita-
109 tion (Kooperman et al. 2018), or remote precipitation by driving changes in large-scale circulation
110 (Swann et al. 2012). These large-scale atmospheric feedbacks to vegetation change can result
111 in remote climate and vegetation responses in regions far removed from the initial vegetation
112 change (Swann et al. 2012; Garcia et al. 2016; Swann et al. 2018). Analysis of the climate impact
113 of changes in vegetation which do not allow for atmospheric feedbacks, such as simulations of
114 changes in vegetation forced with non-interactive data atmospheres (e.g. land models forced with
115 reanalysis) capture the direct surface climate response, but are unable to capture any of the climate
116 response to vegetation change resulting from atmospheric feedbacks.

117 Changes in vegetation have been shown to drive substantial atmospheric responses in many
118 modern ESMs (Gibbard et al. 2005; Bala et al. 2007; Davin et al. 2010; Chen et al. 2012; Medvigy
119 et al. 2013; Devaraju et al. 2015; Badger and Dirmeyer 2015; Swann et al. 2012; Laguë and
120 Swann 2016). However, changing vegetation type in a modern land model encompasses many
121 simultaneous changes to multiple land surface properties, including albedo (through changes in
122 leaf albedo and leaf area), resistance to evaporation (through changes in stomatal conductance
123 and rooting depth), and aerodynamic roughness (through changes in vegetation height). Several
124 studies using early coupled global climate models demonstrated the ability of changes in *individual*
125 surface properties to influence global climate, including albedo (Charney et al. 1975; Charney
126 1975; Charney et al. 1977), roughness (Sud et al. 1988), and land evaporation (Shukla and Mintz
127 2013). However, there has been limited work exploring the individual impact of various land
128 surface properties on climate using modern earth system models (Davin et al. 2010). In many
129 modern land surface models, it can be very difficult to modify only a single property of the land
130 surface; thus, in order to better understand where the atmosphere is most sensitive to a change in
131 the land surface, and what physical surface properties most impact the atmosphere, a simpler land
132 model than those found in most Earth System Models is desirable.

133 In this study, we introduce an idealized land model, the Simple Land Interface Model (SLIM),
134 which we couple to a modern Earth System Model. We use this idealized land model to examine
135 the effects of specified changes in vegetation albedo, evaporative resistance, and surface roughness
136 in uncoupled land-only and in coupled land-atmosphere simulations. These simulations examine
137 climate sensitivity to specific land surface processes, identify different regional climate sensitivity,
138 quantify the impact of atmospheric feedbacks to land surface changes, and provide a quantitative
139 evaluation of how large a surface perturbation is required to achieve a desired change in surface
140 temperature.

141 2. Methods

142 We test the climate response to three properties of the land surface: albedo (how reflective of
143 shortwave radiation a surface is), evaporative resistance (how difficult it is to evaporate water
144 stored in the ground), and vegetation height (how aerodynamically rough the land surface is).

145 *a. Experimental Design*

146 In order to modify a single land surface property, while holding all other properties fixed, we
147 wrote a very simple land surface model (see section b), which can be coupled into the Community
148 Earth System Model (CESM (Hurrell et al. 2013)). This simple land model replaces the Commu-
149 nity Land Model v. 5 (CLM5; (Lawrence et al. 2018)) within CESM; simulations are run coupled
150 to the Community Atmosphere Model v. 5 (CAM5) or a data atmosphere, and a slab ocean model
151 (SOM) (Neale et al. 2012). The slab ocean assumes ocean circulation does not change throughout
152 the simulation (monthly heat fluxes are prescribed for each ocean gridcell, representing horizon-
153 tal and vertical energy transport within the ocean), but allows sea surface temperatures (SSTs)
154 to adjust to forcings from the atmosphere. SOMs allow atmospheric signals to propagate further
155 than fixed SST models, but are much less computationally expensive than fully dynamic ocean
156 models and don't allow for climate signals driven by variability in ocean circulation. As such,
157 the SOM provides a good compromise for studying the impacts of changes in the land surface on
158 atmospheric circulation.

159 In each experiment, we modify the value of a single surface property while holding the rest
160 of the surface properties fixed. For each surface property, we run two sets of simulations: one
161 where the land model is forced with a data atmosphere ('offline'), and one running fully coupled
162 to CAM5 (figure 1). In the offline simulations, we use atmospheric forcing data generated by a
163 control simulation of CAM5 running coupled to the simple land model with the following surface

164 property values, which roughly correspond to a world where all non-glaciated land regions are
165 grasslands: snow-free albedo = 0.2, evaporative resistance = 100 s/m, and vegetation height =
166 10 cm. The offline simulations are all forced with the same 3-hourly atmospheric forcing data
167 saved from this coupled simulation; we find the results to be qualitatively similar when the offline
168 simulations are forced with GSW3P reanalysis, which is the standard atmospheric forcing dataset
169 used to evaluate CLM5 in offline simulations (Lawrence et al. 2018).

170 We perturb the value of each of these surface properties over all non-glaciated (in the present
171 day) land surfaces. For albedo α , we use $\alpha = 0.1$ (comparable to the albedo of a needleleaf
172 evergreen forest), $\alpha = 0.2$ (comparable to the albedo of a grassland), and $\alpha = 0.3$ (comparable to
173 the albedo of a desert) (Bonan 2008a), while holding evaporative resistance fixed at 100 s/m and
174 vegetation height fixed at 0.1 m. For evaporative resistance r_s , we use $r_s = 50\text{s/m}$ (low resistance),
175 $r_s = 100\text{ s/m}$, and $r_s = 200\text{ s/m}$ (moderately high resistance - see Fig. 17.10 in Bonan (2015)), while
176 holding albedo fixed at 0.2 and vegetation height fixed at 0.1 m. For vegetation height h_c (height
177 of canopy) we use $h_c = 0.1\text{ m}$ (short grassland), $h_c = 1.0\text{ m}$ (tall grass), $h_c = 2.0\text{ m}$ (shrub), h_c
178 $= 5.0\text{ m}$ (short tree), $h_c = 10.0\text{ m}$, and $h_c = 20.0\text{ m}$ (moderately tall tree) (Bonan 2008a). We
179 use six experiments for the vegetation height simulations (rather than three as for albedo and
180 evaporative resistance) because its effect on surface fluxes have more potential for non-linearities.
181 Atmospheric forcing data from the fully coupled land-atmosphere simulation with $\alpha = 0.2$, $r_s =$
182 100 s/m , and $h_c = 0.1\text{ m}$ is saved every 3 hours, and used to force the offline simulations.

183 Each simulation is run for 50 years; we discard the first 20 years of the simulation to allow for
184 the model to reach equilibrium, and evaluate the last 30 years of each simulation.

185 *b. Simple Land Interface Model (SLIM)*

186 The simple land model used here (the Simple Land Interface Model, SLIM) allows us to indi-
187 vidually modify different surface properties within a coupled climate model, to isolate their effect
188 on climate. SLIM is described in greater detail in the supplemental materials of this paper.

189 For this study, SLIM was written to couple into CESM in place of CLM. At every land location,
190 the user can independently set each land surface property. These properties include the snow-free
191 albedo, evaporative resistance, vegetation height (for aerodynamic roughness), the capacity of the
192 land to hold water, the heat capacity and thermal resistance of the soil, the number and depth of
193 soil layers, the snow-masking depth (the volume of snow required to mask the snow-free ground
194 albedo), and the locations of glaciers. Hydrology is represented using a bucket model, where the
195 resistance to evaporation from the bucket is a combination of a user-prescribed “lid” resistance
196 (comparable to the bulk stomatal resistance of a complex land model like CLM) and an additional
197 resistance due to how empty the bucket is (as in the GFDL-LM2 model (Milly and Shmakin 2002;
198 Anderson et al. 2004) and Manabe and Bryan (1969)). Given semi-realistic values for albedo,
199 vegetation height, and evaporative resistance, SLIM can qualitatively reproduce the climate of
200 CLM5 using reanalysis atmospheric forcing data (see supplemental figures 2-9).

201 At each time step, the land model solves a linearized surface energy budget to calculate a surface
202 temperature and surface fluxes of radiation, sensible and latent heat flux, and heat uptake by the
203 ground. A simple snow model allows snow falling from the atmosphere to accumulate on the
204 surface and mask the bare ground albedo; snow is removed from the surface either by sublimation
205 to the atmosphere, or by melting into the land surface.

206 *c. Analysis Approaches*

207 For each surface property, we fit a least-squares linear regression model of a climate variable
208 (e.g. surface temperature) to the prescribed values of the surface property (figure 2). Each surface
209 property value has 30 points, one annual mean value for each spun-up simulation year. When
210 fitting our linear model, we track how linear the relationship between the change in global surface
211 property (e.g. albedo in figure 2) and the response of the climate variable in question (surface
212 temperature in figure 2) using the r^2 value of the linear relationship. We test if the slope is signif-
213 icantly different from zero using the p value (where $p < 0.05$ indicates a statistically significant
214 relationship at 95% confidence).

215 In order to evaluate the climate response to physically meaningful changes in each surface prop-
216 erty, we scale the slope by a somewhat arbitrary scaling factor chosen to show a maximum temper-
217 ature change of roughly 1 K in the coupled simulations, which corresponds to maximum surface
218 energy flux changes of approximately 10 W/m². This corresponds to a scaling factor of -0.04 for
219 albedo (the surface gets 4% darker), 50 s/m for evaporative resistance (increasing surface resi-
220 stance), and -5 m for vegetation height (response per 5m shorter/smoothen the surface becomes).
221 For example, a slope of -20 K per 1.0 increase in albedo isn't physically meaningful, as albedo
222 values only range between 0 and 1. Instead, we scale the slope to get a change of -0.8 K (-20
223 K×0.04) per 4% decrease in albedo. In order to evaluate the warming impact of each surface prop-
224 erty, we look at the effects of *decreasing* albedo, *increasing* evaporative resistance, and *decreasing*
225 vegetation height. This slope value is calculated individually for each gridcell, and presented as
226 the climate response to each scaled change in surface property in the rest of the paper.

227 3. Results and Discussion

228 *a. Albedo*

229 The albedo (the fraction of incident radiation that is reflected) of different land surfaces varies
230 greatly between vegetation and land cover types. Coniferous forest albedos range from 0.05-
231 0.15, deciduous forests from 0.15-0.20, grasslands from 0.16-0.26, and soils from 0.05-0.40; snow
232 cover leading to land albedos of over 0.9 (Bonan 2002). We scaled our results so that they are
233 relative to a 0.04 change in land surface albedo; physically, this can be thought of as a conservative
234 approximation of the albedo difference between a coniferous and deciduous forest, or a deciduous
235 forest and a grassland.

236 Albedo directly controls the amount of solar energy absorbed by the land surface, and as such,
237 plays an important role in controlling land surface temperatures. If the land surface absorbs more
238 energy in response to decreasing surface albedo, more energy must also leave the surface, either
239 by an increase in turbulent energy fluxes (sensible and latent heat), or by an increase in longwave
240 radiation emitted by the surface (increasing surface temperature). Over long timescales the storage
241 of energy by the land surface is negligible.

242 1) OFFLINE

243 The differences in the pattern of temperature change in response to albedo in the offline simu-
244 lations, where no atmospheric feedbacks are allowed, are caused by differences in (i) the change
245 in absorbed solar energy (a function of downwelling solar radiation) and (ii) the partitioning of
246 energy into turbulent heat fluxes vs surface heating.

247 In the offline simulations, the temperature response to decreasing land surface albedo is largest
248 in the mid-latitudes, and smallest at high latitudes (figure 3d; supplemental figure 10a). Because

249 the incident sunlight is weaker at high latitudes, the same decrease in surface albedo results in
250 a smaller net increase in absorbed solar radiation compared to lower latitudes. This means that
251 in high latitudes there is less extra energy that the surface needs to get rid of (either through
252 warming or through turbulent heat fluxes), and the total temperature change is small. Conversely,
253 temperature changes in the offline simulations are larger in regions with a large amounts of incident
254 solar radiation at the surface (the tropics and mid-latitudes). Despite the fact that equatorial regions
255 receive the most incoming solar radiation at the top of the atmosphere, the large amount of deep
256 cloud cover over the tropics blocks a lot of solar radiation, and the largest amount of downwelling
257 solar radiation at the surface in the annual mean actually occurs over northern Africa and the
258 Arabian Peninsula (supplemental figure 11).

259 The temperature response to decreasing albedo in the tropics is smaller than in the mid-latitude
260 deserts not only because of the difference in the incident solar radiation at the surface, but also
261 because of differences in the amount of water available on the land surface due to high tropical
262 precipitation rates. As such, though decreasing albedo does lead to an increase in the total energy
263 absorbed at the surface in the tropics (figure 4e), that excess energy is removed from the surface
264 primarily by evaporating more water (figure 4h), negating the need for increased surface tempera-
265 tures and changes in upwards longwave radiation (figure 4f). The largest temperature changes in
266 the offline simulations occur in sunny, dry regions such as the Sahara and Arabian Peninsula where
267 latent cooling is not able to occur and the excess absorbed solar energy is balanced by increased
268 surface temperatures and sensible heat fluxes (figure 4f, g).

269 2) COUPLED

270 In our offline simulations, the climate impact of a change in a land surface property represents
271 the response *independent* of any atmospheric feedbacks. That is, the changes are driven only

272 by the surface energy budget adjustment to the local change in surface property (figure 1a), and
273 not by any change in atmospheric temperature, cloud cover, etc, which may occur due to any
274 interaction with the atmosphere (figure 1b and c). Rather, changes in energy fluxes would be
275 transmitted to the atmosphere, with potential resulting interactions and feedbacks between the
276 land and the atmosphere. Interactions with the atmosphere could cause further changes in surface
277 climate through several pathways, three of which are discussed here. First, changes in atmospheric
278 air temperature could modify the magnitude of downwelling longwave radiation and the surface-
279 to-atmosphere temperature gradient which influences sensible heat flux. Second, changes in cloud
280 cover could modify the magnitude of both downwelling shortwave and longwave radiation at the
281 surface. Third, changes in humidity could modify the vertical moisture gradient which influences
282 latent heat flux.

283 In the coupled simulations, not only is the response of surface temperature to decreasing albedo
284 much larger in magnitude compared with the offline simulations, but it is also drastically different
285 in spatial pattern (figure 3a vs d). Rather than the high latitudes having the smallest temperature
286 response to decreased albedo, they now have some of the largest warming signals (along with
287 hot, dry regions in the mid-latitudes). The magnitude of warming at the surface in the coupled
288 simulations is larger than in the offline simulations in almost all regions, with the exception of
289 equatorial Africa. When the atmosphere is allowed to respond (coupled simulations), decreasing
290 the surface albedo still generally leads to an increase in absorbed shortwave radiation. However,
291 the change in absorbed energy is smaller in magnitude and has a different spatial pattern than in
292 the offline simulations, with near-zero changes in absorbed shortwave radiation in the parts of the
293 tropics and high latitudes, and the largest increases in absorbed solar radiation occurring over the
294 mid-latitudes and parts of tropical South America (compare figure 4a and d). Surprisingly, there
295 are some locations where decreasing albedo actually leads to slightly less absorbed solar radiation

296 at the surface. This response is most notable in the coupled simulation over equatorial Africa,
297 and is the result of increased cloud cover over this region reducing the incident solar radiation
298 (supplemental figure 12). For example, in equatorial Africa the coupled simulations show no
299 change in absorbed solar radiation as surface albedo is decreased, while the offline simulations
300 show a large increase in absorbed solar radiation.

301 Across the tropics, decreasing albedo leads to much larger increases in latent heat flux in the
302 coupled simulations than in the offline simulations, most notably over India, equatorial Africa,
303 Indonesia, and the western Amazon. Many of these regions also stand out as having a decrease
304 in net longwave radiation at the surface, despite surface warming. In these regions, the increases
305 in upwards longwave radiation (a function of surface temperature) are larger than the increases in
306 downwelling longwave radiation associated with atmospheric warming, resulting in the decrease
307 in net longwave radiation at the surface.

308 The increase in annual mean surface temperature at high latitudes is largest in autumn and winter
309 (not shown), when the incoming insolation is very small. This is surprising, as decreasing surface
310 albedo during dark months has a much smaller impact on absorbed shortwave radiation than de-
311 creasing albedo during bright months; moreover, much of the high-latitude land surface is covered
312 with (bright) snow during the winter months, masking the direct change in surface albedo. This
313 suggests that the high-latitude winter warming is not locally driven: there is a significant increase
314 in energy transport into the Arctic region, leading to high-latitude warming driven by changes in
315 energy transport which itself is driven by changes in tropical and mid-latitude albedo (see figure
316 9a as discussed below). Additionally, there is significant loss of sea ice (largest in September) for
317 the reduced albedo simulations, corresponding to a large warming signal over the entire Arctic
318 Ocean region (supplemental figure 13).

319 *b. Evaporative Resistance*

320 Vegetation can directly control the evaporative resistance of a surface through the opening and
321 closing of stomata on their leaves. The evaporative resistance of a surface is also controlled by soil
322 properties, vegetation root depth, and how much water is available in the soil. Here, we present
323 results for a 50 s/m change in the evaporative resistance of the land surface. The total resistance
324 to evaporation is a combination of the surface resistance (which we perturb) and the resistance
325 associated with how dry the soil is. Changing the evaporative resistance of the land surface has
326 no direct effect on the total amount of energy absorbed by the surface; rather, it controls the
327 partitioning between latent and sensible heat fluxes (figure 5). In general we expect that a surface
328 with higher resistance would have relatively more sensible and less latent heat flux, leading to
329 higher surface temperatures relative to a surface with lower resistance.

330 1) OFFLINE

331 Our offline simulations show the largest change in surface temperature in the wettest regions
332 of the tropics (figure 3e). This response is intuitive: increasing resistance in these regions causes
333 a large reduction in latent heat flux (figure 5h), which is compensated for by surface warming,
334 increased sensible heat flux, and increased upwards longwave radiation (figure 5f, g). Dry re-
335 gions (e.g. the Sahara and central Australia) have no temperature response to increasing surface
336 resistance in the offline simulations: these regions have very little water on the land surface and
337 near-zero latent heat fluxes, so making it more difficult to evaporate water does not result in any
338 substantial changes to the actual magnitude of latent heat flux, and thus there is no compensating
339 change in the other terms of the surface energy budget. The amount of shortwave radiation ab-
340 sorbed at the surface is only a function of the downwelling shortwave radiation and the albedo of
341 a surface; as such, increasing evaporative resistance in offline simulations has no impact on the

342 absorbed solar energy at the surface (figure 5e). Instead, evaporative resistance directly controls
343 the partitioning of energy between turbulent heat fluxes.

344 2) COUPLED

345 As with albedo, the pattern and magnitude of the surface temperature response to increasing
346 evaporative resistance over land have a larger magnitude and a spatially distinct pattern in our
347 coupled simulations compared to their offline counterparts (figure 3b). Rather than in the wettest
348 tropical regions, our coupled simulations have the largest changes in surface temperature in re-
349 sponse to decreasing surface resistance in the mid-to-high latitudes. Dry regions in the subtropics
350 have the smallest change in surface temperature when evaporative resistance is increased, but these
351 regions still show more warming than in the offline simulations.

352 One of the largest changes in surface temperature in response to increased evaporative resistance
353 occurs over southeastern North America. Over this region, there is a slight decrease in evaporation
354 in both the coupled and offline simulations (compare figure 5d and h). However, the changes to
355 temperature and energy fluxes are otherwise quite different. In the coupled simulation, increased
356 evaporative resistance at the land surface drives warming and drying of the regional atmosphere.
357 The warming and drying of the lower troposphere in this region leads to a decrease in relative
358 humidity and a decrease in low cloud cover (not shown). The reduction in cloud cover in turn
359 allows more solar radiation to reach the surface, causing surface temperatures to rise. Averaged
360 over the region from 85 to 100° W and 32 to 45 °N, a 50 s/m increase in evaporative resistance
361 leads to a 6.2 W/m² in absorbed solar radiation in the coupled simulations. This increase in
362 energy into the land system over this region results in a temperature increase of roughly 0.9 K
363 in the coupled simulation, compared to a warming of only 0.2 K in the uncoupled simulation
364 (per 50 s/m increase in evaporative resistance). This cloud feedback is particularly interesting

365 as evaporative resistance cannot directly modify the amount of energy absorbed by the surface.
366 However, when the atmosphere is allowed to respond to the decrease in latent heat flux driven
367 by increased evaporative resistance, cloud feedbacks result in an increase in downwelling solar
368 radiation, and thus an increase in net absorbed solar radiation despite there being no change in
369 surface albedo.

370 *c. Roughness*

371 1) OFFLINE

372 Changing the height of vegetation changes the aerodynamic roughness of the land surface, and
373 thus how effectively turbulent energy fluxes can be exchanged with the atmosphere. Decreasing
374 surface roughness makes it harder to remove energy from the land surface by turbulent mixing; as
375 such, it leads to a reduction in sensible heat flux, with an equal and opposite increase in longwave
376 radiation corresponding to an increase in surface temperature, with little to no impact on latent heat
377 flux (figure 6f-h). Roughness has no direct effect on albedo, and thus in the offline simulations has
378 no impact on the amount of energy being absorbed by the land (figure 6e).

379 2) COUPLED

380 Unlike decreasing albedo and increasing evaporative resistance, which result in larger temper-
381 ature changes with different spatial patterns in the coupled compared to the offline simulations,
382 decreasing surface roughness results in a similar pattern of warming in the coupled vs offline
383 simulations. Moreover, the warming is actually weaker in the coupled simulations (figure 3c, f).

384 This occurs because in the coupled simulations, the atmosphere can respond to the change in
385 surface fluxes by changing temperature aloft. For a given surface roughness, the magnitude of
386 the sensible heat flux is a function of the temperature difference between the air in the lowest

387 level of the atmosphere and the surface temperature. In the coupled simulations, the air in the
388 lowest level of the atmosphere can change temperature in response to forcing from the surface,
389 while in the offline simulations, the air temperature visible to the land model is unaffected by any
390 changes to the land surface. The air in the lowest level of the atmosphere warms as the surface
391 becomes smoother. With all else held equal, this reduces the temperature gradient between the
392 surface and the atmosphere, thus resulting in smaller changes to sensible heat fluxes, and thus
393 smaller changes to longwave radiation (which balance the change in sensible heat flux as surface
394 roughness changes).

395 In both the offline and coupled experiments, decreasing the vegetation height (and thus the
396 surface roughness) has the largest impact on temperature in the warmest regions of the globe,
397 with much smaller annual mean temperature increases in the high latitudes. As the roughness of a
398 surface should impact how efficiently turbulent heat can be moved away from the surface, it should
399 have the largest impact on surface temperatures in regions where turbulent heat fluxes play a large
400 role in balancing the surface energy budget.

401 During winter in the high latitudes, air temperatures can be substantially warmer than surface
402 temperatures; as such, decreasing surface roughness, which decreases turbulent heat exchange,
403 actually leads to a cooling of the surface (supplemental figure 14), rather than the more typical
404 warming effect, as turbulent mixing of sensible heat actually moves warm air from the atmosphere
405 down to the surface in these regions. In the coupled simulations, where temperatures in the lower
406 atmosphere can adjust to surface temperatures, this response is not significant. However, in the
407 offline simulations where lower atmospheric temperatures are held fixed, this mechanism causes
408 surface smoothing to drive large cooling signal over high northern latitudes. This (wintertime)
409 cooling in the offline simulations drives the sign difference in the amount of warming coming
410 from the atmosphere (figure 7c).

411 *d. Feedbacks*

412 In the real world, as well as in our coupled simulations, the land surface does not respond
413 to forcing in isolation – changes in surface energy fluxes are communicated to the atmosphere,
414 and can drive changes in atmospheric temperature, humidity, cloud cover, and circulation as noted
415 above. Many of these atmospheric responses to changes in surface energy fluxes can then feedback
416 on the surface energy budget itself. For example, a change in cloud cover driven by some initial
417 surface change could lead to a subsequent change in solar radiation reaching the surface, which in
418 turn drives further changes in the surface energy budget (figure 1b). Additionally, the atmosphere
419 can transmit information (e.g. changes in circulation, or fluxes of water, heat, or clouds) from one
420 atmospheric column to another, such that a change in the land surface in one region can, through
421 these remote atmospheric feedbacks, influence the surface energy budget in a remote region (figure
422 1c).

423 1) TOTAL ATMOSPHERIC FEEDBACK

424 The differing surface fluxes between simulations where the atmosphere is or is not allowed to re-
425 spond result in remarkably different patterns and magnitudes of surface temperature change for the
426 same imposed surface property change as described above (figure 3). Because the atmosphere can
427 respond to changes in surface fluxes, modifying land albedo, evaporative resistance, and roughness
428 can lead to large changes in cloud cover, snow fall, sea ice, and energy transport, all of which can
429 feedback on the surface energy fluxes over the land surface.

430 We define the total *atmospheric feedback* on surface climate to be the difference between the
431 coupled simulation and the offline simulation (figure 7 – for surface air temperature, this would
432 be the difference between the left and right columns of figure 3). For albedo and evaporative
433 resistance, the extra-tropics have up to 1K of additional surface warming when the atmosphere

434 is allowed to respond to changes in surface energy fluxes driven by the modified land surface
435 properties.

436 To identify the strength of the atmospheric feedback – that is, what percent of the total warming
437 signal comes from interactions with the atmosphere – we calculate the percent change in a surface
438 temperature between the coupled simulation and the offline simulation:

$$\text{Feedback Strength} = \frac{\text{coupled} - \text{offline}}{|\text{coupled}|} \times 100. \quad (1)$$

439 For albedo, over 50% of the change in surface temperature comes from interactions with the at-
440 mosphere over more than 80% of global, non-glaciated land area, with as much as 75% of the
441 temperature response coming from the atmosphere over 28% of land area. This is even larger
442 for evaporative resistance, over 50% of the surface temperature increase comes from atmospheric
443 feedbacks over 84% of non-glaciated land areas, with increases as large as 75% over 64% of land
444 area (figure 8). This suggests that vegetation changes which significantly alter either the color of
445 the land surface, or how difficult it is to remove water from the land surface (such as the conver-
446 sion of a forest to a grassland) have significant impacts on surface climate *due to* changes in the
447 atmosphere in response to the initial vegetation change – changes which cannot be captured by an
448 offline land model simulation.

449 2) IMPACT ON GLOBAL ATMOSPHERIC CIRCULATION

450 In addition to changes in temperature driven by changes to the local surface energy budget,
451 decreasing albedo and increasing evaporative resistance both drive changes in large-scale atmo-
452 spheric circulation, evident by a significant change in northward energy transport by the atmo-
453 sphere (figure 9a). When excess energy is absorbed in the northern hemisphere the Hadley Circu-
454 lation shifts to move energy from the energy rich northern hemisphere to the southern hemisphere,
455 causing the intertropical convergence zone to shift towards the energy rich hemisphere (figure 9b).

456 This response is well documented in slab ocean models (Chiang and Bitz 2005; Kang et al. 2008;
457 Swann et al. 2012; Frierson and Hwang 2012; Chiang and Friedman 2012; Laguë and Swann
458 2016) and also found in models with dynamical oceans (Broccoli et al. 2006). If such an energy
459 gradient is established, we expect to see this large-scale circulation response.

460 In the case of albedo, a darker surface directly increases the amount of energy absorbed by the
461 land surface. Because the northern hemisphere has more land – in particular, more non-glaciated
462 land (we only modify non-glaciated land in this study) – than the southern hemisphere, decreasing
463 land albedo globally results in more energy being absorbed by the surface in the northern hemi-
464 sphere than in the southern hemisphere. The resulting energy gradient causes a southward shift
465 in the Hadley Circulation, evident in the increased southward energy transport across the equator.
466 However, decreasing land albedo also has the effect of slightly increasing the energy transport
467 from the northern mid-latitudes into the Arctic, leading to high-latitude warming *driven* by the
468 non-local albedo changes in the tropics and mid-latitudes.

469 Evaporative resistance, unlike albedo, does not directly change the amount of energy absorbed
470 by the surface – rather, it changes the partitioning of energy between sensible and latent heat. As
471 such, it is surprising that increasing evaporative resistance drives a large, significant decrease in
472 northward energy transport (blue line in figure 9a). We find that increasing evaporative resistance
473 drives a decrease in cloud cover over many land areas; this causes an increase in downwelling
474 shortwave radiation at the surface, and thus an increase in net shortwave energy absorbed at the
475 surface despite no change in surface albedo (supplemental figure 12b, figure 5a). This introduces
476 the hemispheric energy imbalance required to drive the observed large-scale shifts in energy trans-
477 port.

478 Changing the roughness of the surface has only a weak impact on the total amount of energy
479 absorbed by the land, and as such we see only small changes in northward energy transport and
480 zonal mean precipitation (orange lines in figure 9).

481 3) RESPONSE OVER OCEANS

482 Changes in land surface properties drive changes in surface climate not only over the land,
483 but also over the oceans. The slab ocean model employed in these simulations allows sea surface
484 temperatures (SSTs) and sea surface energy fluxes to respond to changes in the atmosphere (though
485 heat transport within the ocean is held fixed). As such, atmospheric signals *driven by changes in*
486 *the land surface* can propagate over the oceans, impacting SSTs, oceanic clouds, and precipitation,
487 and potentially reaching far-removed land surfaces. Unlike the climate response over land regions
488 in the fully coupled simulations, where the change in climate may be coming directly from the
489 change in the land surface at that grid cell, or from atmospheric responses to remote changes in
490 the land surface, the climate response over the ocean must inherently be a remote response to
491 changes in the land surface, given that the ocean surface was not directly modified in any of our
492 simulations.

493 When we make the land surface darker (reduce albedo), there is a large warming response over
494 the Arctic Ocean, caused by a strong sea ice feedback where arctic warming leads to loss of sea
495 ice, which amplifies high-latitude warming (figure 11). The warming which initially drives the
496 sea ice loss is a combination of both local warming from land in the northern high-latitudes, as
497 well as from an increase in energy transport into the high northern latitudes (figure 9a). With
498 a darker land surface, the increase in absorption of solar radiation over land drives increased air
499 temperatures over land; this warming is then advected by the atmosphere, resulting most notably in
500 increased SSTs downwind of land masses in the northern hemisphere. In contrast to the northern

501 hemisphere warming over the oceans, in the southern hemisphere the temperature response over
502 the cloud decks west of South America, southern Africa, and Australia are near-zero or negative.
503 This cooling is caused by an increase in low cloud cover over these regions, which in turn is
504 supported by increase subsidence over these low cloud decks (supplemental figure 15). Whether
505 the increased subsidence is due to the direct albedo change of the neighboring continent (e.g.
506 setting up a local East-West, Walker-like circulation), or is driven by the changes in large-scale
507 atmospheric circulation (e.g. increased subsidence as a result of a shifting ITCZ), would require
508 further simulations and is not the focus of this study.

509 *e. Inverse relationship*

510 Thus far, we have considered the response of various climate variables (e.g. T_s , the surface en-
511 ergy budget, clouds) as the change in that climate variable per incremental change in the magnitude
512 of a surface property (albedo, evaporative resistance, or roughness); that is, we have considered the
513 slope $\frac{\partial \text{atm}}{\partial \text{Ind}}$. However, in order to compare the relative impact of changes in different surface prop-
514 erty types it would be useful to know how much of a change in each property is needed to cause
515 the same amount of temperature response. We can use our simulations to consider the inverse
516 relationship $\frac{\partial \text{Ind}}{\partial \text{atm}}$. By scaling $\frac{\partial \text{Ind}}{\partial \text{atm}}$ such that $\partial \text{atm} = 0.1 \text{ K}$, this relationship can be interpreted
517 as the magnitude of global change in some surface property (albedo, evaporative resistance, or
518 roughness) required to drive a 0.1 K increase in surface temperature at any particular location (fig-
519 ure 10). A similar calculation can be applied to the offline simulations, which *do not account* for
520 any atmospheric feedbacks; in that case, we calculate the local change in surface albedo required
521 to drive an 0.1 K change in local surface temperature, with no interaction effects from the local
522 atmosphere, and no temperature effects from remote albedo change.

523 In the coupled simulations, only a small change (< 0.0005) in global land surface albedo is
524 required to drive 0.1K of warming over 93.2% of land areas (figure 10a). This is well within the
525 range of actual surface albedo changes associated with vegetation change, with grass albedos alone
526 ranging from 0.16-0.26 (Bonan 2002). In the offline simulations, only 18.5% of land areas achieve
527 an 0.1K warming with an albedo change of < 0.0005 in the offline simulations (figure 10d).

528 To achieve an 0.1K temperature increase at any given location from global-scale changes in
529 evaporative resistance, quite large increases in global evaporative resistance would be required
530 (figure 10b). For example, to see 0.1K of warming over southwestern North America, a roughly
531 400 s/m increase in global land evaporative resistance would be required - a value larger than
532 the difference in evaporative resistance of a wheat field to a forest (Bonan 2015). It should also
533 be noted that this type of analysis necessarily assumes linearity, and that the ranges of change in
534 evaporative resistance required to drive an 0.1K warming are larger than the range tested (200 s/m)
535 in 98% of land areas. The offline simulations require physically unrealistically large changes in
536 global land evaporative resistance to drive an 0.1K local temperature (figure 10b), largely because
537 the warming in response to increased evaporative resistance is due to atmospheric feedbacks. Only
538 in some very wet areas, such as Indonesia, does a change in evaporative resistance translate to a
539 substantial temperature change in the offline simulations. Indeed, in many regions (blue in figure
540 10e), the relationship between increasing evaporative resistance and surface warming is actually
541 negative (but also very weak).

542 Decreasing global land surface vegetation height by < 5.0 m leads to 0.1K of surface temperature
543 change over roughly 33% (41%) of land areas in the coupled (offline) simulations. Modifying
544 the surface roughness can lead either to warming or cooling, with smoother surfaces leading to
545 warming at lower latitudes, and smoother surfaces leading to cooling at high latitudes (where the
546 air is frequently warmer than the surface, particularly during winter, thus turbulent mixing would

547 act to warm rather than cool the surface). Because atmospheric feedbacks play a smaller role in
548 the local climate impact of changing vegetation height, the offline map can be interpreted as an
549 indicator of where a local change in surface roughness is likely to result in a substantial change in
550 local surface temperature.

551 *f. Caveats and Limitations*

552 In this study we have established that the feedbacks from the atmosphere are large, comprising
553 for example 75% or more of the total response of surface temperature to a change in surface
554 resistance over 64% of land area. However, atmospheric feedbacks can be local (a change in the
555 atmosphere above some location due to a change in land properties at that location) or remote (a
556 change in the atmosphere above some location due to a change in land properties at a different
557 location). We can see this effect clearly over the oceans where the climate response must be
558 entirely remote, as the surface of the ocean is never directly modified in this study. However
559 with our simulations alone, we cannot fully separate the effects of local vs. remote atmospheric
560 feedbacks over land because all land areas are perturbed at the same time; doing so will be left for
561 future studies.

562 We present the response of surface fluxes and temperatures to changes in different land sur-
563 face properties. However, the change in the 2m air temperature does not necessarily mirror the
564 change in the *surface* (radiative) temperature of the land surface. This is particularly evident when
565 comparing the effect of changes in roughness on surface vs 2m air temperature (figure 11); while
566 albedo and evaporative resistance result in warming both of the land surface and the air in the cou-
567 pled simulations, the magnitude of surface temperature response to decreasing roughness is much
568 larger than that of 2m air temperature.

569 In this study we aim to isolate the effect of individual surface properties on climate, and so in
570 each experiment we modify a single land property at a time. When considering the climate impact
571 of actual land use change, for example changing from a forest to a grassland, multiple properties
572 of the land surface are changed simultaneously. It is possible that modifying multiple surface
573 properties at the same time and in different patterns leads to non-linear responses which we have
574 not addressed in the results presented here. Additionally, the strength of the atmospheric feedbacks
575 presented here are the results on a single atmospheric model (CAM5); other atmospheric models
576 could show stronger or weaker responses to changes in the land surface, particularly with regards
577 to cloud cover.

578 **4. Summary and Conclusions**

579 We evaluated the sensitivity of climate over the land surface to changes in three individual land
580 surface properties (albedo, evaporative resistance, and aerodynamic roughness). Changes in land
581 albedo result in more absorbed incoming shortwave radiation, which leads to large surface temper-
582 atures changes in water-limited regions; temperature changes are small, but changes in latent heat
583 flux are large, in regions with ample terrestrial water availability. Albedo has the largest impact
584 on surface temperatures in warm, sunny regions in the offline simulations, but much larger and
585 spatially broader impacts on surface temperatures across the mid and high latitudes in the coupled
586 simulations due to large-scale interactions with the atmosphere. Changes in evapotranspiration do
587 not directly effect the amount of energy absorbed by the surface; rather, changes in evapotranspi-
588 ration lead to changes in the partitioning between sensible and latent heat fluxes, with increased
589 surface temperatures and reduced evaporation when evaporative resistance is increased. Not sur-
590 prisingly, changes in evaporative resistance have the largest impact on surface temperature in wet
591 areas such as the tropics in the offline simulations, with even larger surface temperature responses

592 in the coupled simulations in extratropical regions with both wet soil and relatively dry air, such
593 as south-eastern North America and northern Eurasia. Changes in vegetation height modify the
594 aerodynamic resistance of the land surface, and results in a repartitioning of surface energy fluxes
595 between turbulent heat fluxes - mostly sensible heat flux - and emitted surface longwave radiation
596 (corresponding to changes in surface temperature). Changes in surface roughness have the largest
597 impact on surface temperatures in warm, dry regions.

598 Davin et al. (2010) (hereafter D2010) used a global climate model to explore the effects of
599 global deforestation. Our results are consistent with D2010 that increases global land surface
600 albedo lead to global-scale cooling; the largest temperature changes in their study occur at high lat-
601 itudes, while our largest temperature changes occur in mid-latitudes. Additional differences could
602 result both from the spatially non-uniform surface changes used in D2010, as well as from model-
603 dependency of results. Our work builds upon D2010 in two notable ways: first, by exploring the
604 scaling relationship between different magnitudes of change in albedo, evaporative resistance, or
605 vegetation height and the resulting climate effect, and second, by quantifying how much of the
606 climate response to global changes in each land surface property was the result of atmospheric
607 feedbacks.

608 When investigating the climate effect of changes in land surface properties, the results are dras-
609 tically different between offline land-only simulations driven by non-interactive atmospheric data,
610 and simulations which account for interactions and feedbacks with the atmosphere. The response
611 of surface temperature to changes in albedo and evaporative resistance are much stronger and have
612 a distinctly different pattern in coupled simulations than offline simulations, with over 50% of the
613 total temperature change in response to albedo coming from interactions with the atmosphere in
614 over 80% of land areas. For surface roughness, the pattern and magnitude of temperature change
615 are similar, though not identical, between the coupled and offline simulations. The differences in

616 climate response to the same change in the land surface between the coupled and offline simula-
617 tions come from atmospheric feedbacks responding to surface property-driven changes in surface
618 energy fluxes. These atmospheric feedbacks include changes in atmospheric temperature, humid-
619 ity, cloud cover (which go on to modify the amount of solar radiation reaching the surface), and
620 circulation. Some of these circulation responses, such as changes in northward heat transport, are
621 large in spatial scale and thus provide a mechanism for surface property changes in one location
622 to impact climate over far removed land areas.

623 The inverse relationship presented in this paper describes the change in some land surface prop-
624 erty required to produce a change in a given climate variable, for example, the change in albedo
625 required to drive 1K of surface warming at some location. This approach provides a framework to
626 analyze the impacts of land management on different aspects of surface climate. This highlights
627 the importance of accounting for local land-atmosphere interaction impacts on climate, and for
628 quantifying the impacts of remote land use change on the climate of given region when consider-
629 ing the climate impacts of land management in the future.

630 The simple land model, SLIM, introduced in this paper provides the ideal framework to assess
631 atmospheric responses to prescribed surface perturbations. It allows us to quantify the climate
632 impacts of individual land surface properties while knowing exactly what is changing on the land
633 surface. We foresee this model being useful in applications such as paleoclimate studies where
634 the exact distribution and behavior of vegetation is unknown, studies where the complexity of a
635 modern land surface model is not needed, or studies where unexpected feedbacks with complex
636 land dynamics could interfere with the intended experiments.

637 *Acknowledgments.* We thank funding support from NSF grant 1553715 to the Univer-
638 sity of Washington, NSERC grant PGSD3-487470-2016, and the Advanced Studies Pro-

639 gram visiting graduate student fellowship at the National Center for Atmospheric Research
640 (2016). We would like to acknowledge high-performance computing support from Cheyenne
641 (doi:10.5065/D6RX99HX) provided by NCAR’s Computational and Information Systems Labo-
642 ratory, sponsored by the National Science Foundation. The SLIM (Simple Land Interface Model)
643 source code is available on github at <https://github.com/marysa/SimpleLand> (*this reposi-*
644 *tory is currently private, but can be made available to reviewers and will be made public upon*
645 *publication of this paper*). The data presented in this paper will be archived through Research
646 Works, the University of Washington Libraries digital repository, upon publication of this paper.

647 **References**

- 648 Anderson, J. L., and Coauthors, 2004: The new GFDL global atmosphere and land model AM2-
649 LM2: Evaluation with prescribed SST simulations. *Journal of Climate*, **17** (24), 4641–4673,
650 doi:10.1175/JCLI-3223.1, URL <http://dx.doi.org/10.1175/JCLI-3223.1>.
- 651 Badger, A. M., and P. A. Dirmeyer, 2015: Climate response to Amazon forest replacement by
652 heterogeneous crop cover. *Hydrology and Earth System Sciences*, **19** (11), 4547–4557, doi:
653 10.5194/hess-19-4547-2015.
- 654 Bala, G., K. Caldeira, M. Wickett, T. J. Phillips, D. B. Lobell, C. Delire, and A. Mirin, 2007: Com-
655 bined climate and carbon-cycle effects of large-scale deforestation. *Proceedings of the National*
656 *Academy of Sciences*, **104** (16), 6550–6555, doi:10.1073/pnas.0608998104.
- 657 Boisier, J. P., and Coauthors, 2012: Attributing the impacts of land-cover changes in temperate
658 regions on surface temperature and heat fluxes to specific causes: Results from the first LUCID
659 set of simulations. *Journal of Geophysical Research Atmospheres*, **117** (12), 1–16, doi:10.1029/
660 2011JD017106.

- 661 Bonan, G., 2015: *Ecological climatology: concepts and applications*. 3rd ed., Cambridge Univer-
662 sity Press.
- 663 Bonan, G. B., 2002: *Ecological climatology: concepts and applications*. 1st ed., Cambridge Uni-
664 versity Press.
- 665 Bonan, G. B., 2008a: Ecological Climatology: Concepts and Applications, 2nd Edition. *Geo-*
666 *graphical Research*, **48 (2)**, 221–222, doi:10.1111/j.1745-5871.2009.00640.x, URL <http://doi.wiley.com/10.1111/j.1745-5871.2009.00640.x>.
- 667
- 668 Bonan, G. B., 2008b: Forests and climate change: forcings, feedbacks, and the climate
669 benefits of forests. *Science (New York, N.Y.)*, **320 (5882)**, 1444–1449, doi:10.1126/science.
670 1155121, URL <http://www.ncbi.nlm.nih.gov/pubmed/18556546><http://science.sciencemag.org/content/320/5882/1444.abstract>.
- 671
- 672 Broccoli, A. J., K. a. Dahl, and R. J. Stouffer, 2006: Response of the ITCZ to Northern Hemisphere
673 cooling. *Geophysical Research Letters*, **33 (1)**, 1–4, doi:10.1029/2005GL024546.
- 674 Canadell, J. G., and M. R. Raupach, 2008: Managing forests for climate change mitigation. *Sci-*
675 *ence*, **320 (5882)**, 1456–1457, doi:10.1126/science.1155458.
- 676 Charney, J., W. J. Quirk, S.-h. S.-H. Chow, and J. Kornfield, 1977: A Comparative Study of the
677 Effects of Albedo Change on Drought in Semi–Arid Regions. *Journal of the Atmospheric Sci-*
678 *ences*, **34 (9)**, 1366–1385, doi:10.1175/1520-0469(1977)034<1366:ACSOTE>2.0.CO;2, URL
679 [http://dx.doi.org/10.1175/1520-0469\(1977\)034{\%}3C1366:ACSOTE{\%}3E2.0.CO;2](http://dx.doi.org/10.1175/1520-0469(1977)034{\%}3C1366:ACSOTE{\%}3E2.0.CO;2).
- 680 Charney, J., P. H. Stone, and W. J. Quirk, 1975: Drought in the sahara: a biogeophysical feedback
681 mechanism. *Science (New York, N.Y.)*, **187 (4175)**, 434–435, doi:10.1126/science.187.4175.434.

682 Charney, J. G., 1975: Dynamics of Deserts and Drought in Sahel. *Quarterly Journal of the Royal*
683 *Meteorological Society*, **101 (428)**, 193–202, doi:10.1002/qj.49710142802, URL [http://dx.doi.](http://dx.doi.org/10.1002/qj.49710142802)
684 [org/10.1002/qj.49710142802](http://dx.doi.org/10.1002/qj.49710142802){\%}5Cnpapers2://publication/doi/10.1002/qj.49710142802.

685 Chen, G. S., M. Notaro, Z. Liu, and Y. Liu, 2012: Simulated local and remote biophysical effects
686 of afforestation over the Southeast United States in boreal summer. *Journal of Climate*, **25 (13)**,
687 4511–4522, doi:10.1175/JCLI-D-11-00317.1.

688 Chiang, J. C., and A. R. Friedman, 2012: Extratropical Cooling, Interhemispheric Thermal Gra-
689 dients, and Tropical Climate Change. *Annual Review of Earth and Planetary Sciences*, **40 (1)**,
690 383–412, doi:10.1146/annurev-earth-042711-105545, URL [http://www.annualreviews.org/doi/](http://www.annualreviews.org/doi/10.1146/annurev-earth-042711-105545)
691 [10.1146/annurev-earth-042711-105545](http://www.annualreviews.org/doi/10.1146/annurev-earth-042711-105545).

692 Chiang, J. C. H., and C. M. Bitz, 2005: Influence of high latitude ice cover on the marine Intertrop-
693 ical Convergence Zone. *Climate Dynamics*, **25 (5)**, 477–496, doi:10.1007/s00382-005-0040-5.

694 Davin, E. L., N. de Noblet-Ducoudré, N. de Noblet-Ducoudre, N. de Noblet-Ducoudré, and
695 N. de Noblet-Ducoudre, 2010: Climatic Impact of Global-Scale Deforestation: Radiative ver-
696 sus Nonradiative Processes. *Journal of Climate*, **23 (1)**, 97–112, doi:10.1175/2009JCLI3102.1,
697 URL <http://journals.ametsoc.org/doi/abs/10.1175/2009JCLI3102.1>.

698 Devaraju, N., G. Bala, and A. Modak, 2015: Effects of large-scale deforestation on
699 precipitation in the monsoon regions: Remote versus local effects. *Proceedings of*
700 *the National Academy of Sciences*, **112 (11)**, 201423 439, doi:10.1073/pnas.1423439112,
701 URL <http://www.pnas.org/content/early/2015/02/23/1423439112>[http://www.pnas.org/content/](http://www.pnas.org/content/early/2015/02/23/1423439112)
702 [early/2015/02/23/1423439112](http://www.pnas.org/content/early/2015/02/23/1423439112).full.pdf.

703 Frierson, D. M. W., and Y.-T. T. Hwang, 2012: Extratropical influence on ITCZ shifts in slab
704 ocean simulations of global warming. *Journal of Climate*, **25** (2), 720–733, doi:10.1175/
705 JCLI-D-11-00116.1.

706 Garcia, E. S., A. L. S. Swann, J. C. Villegas, D. D. Breshears, D. J. Law, S. R. Saleska, and S. C.
707 Stark, 2016: Synergistic ecoclimate teleconnections from forest loss in different regions struc-
708 ture global ecological responses. *PLoS ONE*, **11** (11), 1–12, doi:10.1371/journal.pone.0165042.

709 Gibbard, S., K. Caldeira, G. Bala, T. J. Phillips, and M. Wickett, 2005: Climate effects of
710 global land cover change. *Geophysical Research Letters*, **32** (23), L23 705, doi:10.1029/
711 2005GL024550.

712 Hurrell, J. W., and Coauthors, 2013: The community earth system model: A framework for col-
713 laborative research. *Bulletin of the American Meteorological Society*, **94** (9), 1339–1360, doi:
714 10.1175/BAMS-D-12-00121.1.

715 Kang, S. M., I. M. Held, D. M. W. Frierson, and M. Zhao, 2008: The response of the ITCZ
716 to extratropical thermal forcing: Idealized slab-ocean experiments with a GCM. *Journal of*
717 *Climate*, **21** (14), 3521–3532, doi:10.1175/2007JCLI2146.1.

718 Kooperman, G. J., Y. Chen, F. M. Hoffman, C. D. Koven, K. Lindsay, M. S. Pritchard, A. L.
719 Swann, and J. T. Randerson, 2018: Forest response to rising CO₂ drives zonally asym-
720 metric rainfall change over tropical land. *Nature Climate Change*, **8**, 434–440, doi:10.1038/
721 s41558-018-0144-7, URL <http://dx.doi.org/10.1038/s41558-018-0144-7>
722 <http://www.cesm.ucar.edu/events/wg-meetings/2017/presentations/bgcwg+lmwg/kooperman.pdf>.

723 Laguë, M. M., and A. L. S. Swann, 2016: Progressive Midlatitude Afforestation: Im-
724 pacts on Clouds, Global Energy Transport, and Precipitation. *Journal of Climate*,

725 **29** (15), 5561–5573, doi:10.1175/JCLI-D-15-0748.1, URL <http://journals.ametsoc.org/doi/10.1175/JCLI-D-15-0748.1>
726 <http://dx.doi.org/10.1175/JCLI-D-15-0748.1>
727 <http://journals.ametsoc.org/doi/abs/10.1175/JCLI-D-15-0748.1?af=R>.

728 Lawrence, D., and Coauthors, 2018: Technical Description of version 5.0 of the Community Land
729 Model (CLM). Tech. rep., National Center for Atmospheric Research, Boulder, Colorado.

730 Lee, X., and Coauthors, 2011: Observed increase in local cooling effect of de-
731 forestation at higher latitudes. *Nature*, **479** (7373), 384–387, doi:10.1038/
732 nature10588, URL <http://dx.doi.org/10.1038/nature10588>
733 <http://files/1142/Leeetal.-2011-Observedincreaseinlocalcoolingeffectofdefor.pdf>.

734 Manabe, S., and K. Bryan, 1969: Climate Calculations with a Combined Ocean-Atmosphere
735 Model. URL [http://journals.ametsoc.org/doi/abs/10.1175/1520-0469\(1969\)026\(0786:CCWACO\)2.0.CO;2](http://journals.ametsoc.org/doi/abs/10.1175/1520-0469(1969)026(0786:CCWACO)2.0.CO;2),
736 786–789 pp., doi:
737 10.1175/1520-0469(1969)026(0786:CCWACO)2.0.CO;2.

738 Medvigy, D., R. L. Walko, M. J. Otte, and R. Avissar, 2013: Simulated changes in Northwest
739 U.S. Climate in response to Amazon deforestation. *Journal of Climate*, **26** (22), 9115–9136,
740 doi:10.1175/JCLI-D-12-00775.1.

741 Milly, P. C. D., and a. B. Shmakin, 2002: Global Modeling of Land Water and
742 Energy Balances. Part I: The Land Dynamics (LaD) Model. *Journal of Hydrometeorology*, **3** (3), 283–299, doi:10.1175/1525-7541(2002)003(0283:GMOLWA)2.0.CO;
743 2, URL [http://journals.ametsoc.org/doi/abs/10.1175/1525-7541\(2002\)003\(0283:GMOLWA\)2.0.CO;2](http://journals.ametsoc.org/doi/abs/10.1175/1525-7541(2002)003(0283:GMOLWA)2.0.CO;2),
744 2, URL [http://journals.ametsoc.org/doi/abs/10.1175/1525-7541\(2002\)003\(0283:GMOLWA\)2.0.CO;2](http://journals.ametsoc.org/doi/abs/10.1175/1525-7541(2002)003(0283:GMOLWA)2.0.CO;2),
745 2, URL [http://journals.ametsoc.org/doi/abs/10.1175/1525-7541\(2002\)003\(0283:GMOLWA\)2.0.CO;2](http://journals.ametsoc.org/doi/abs/10.1175/1525-7541(2002)003(0283:GMOLWA)2.0.CO;2).

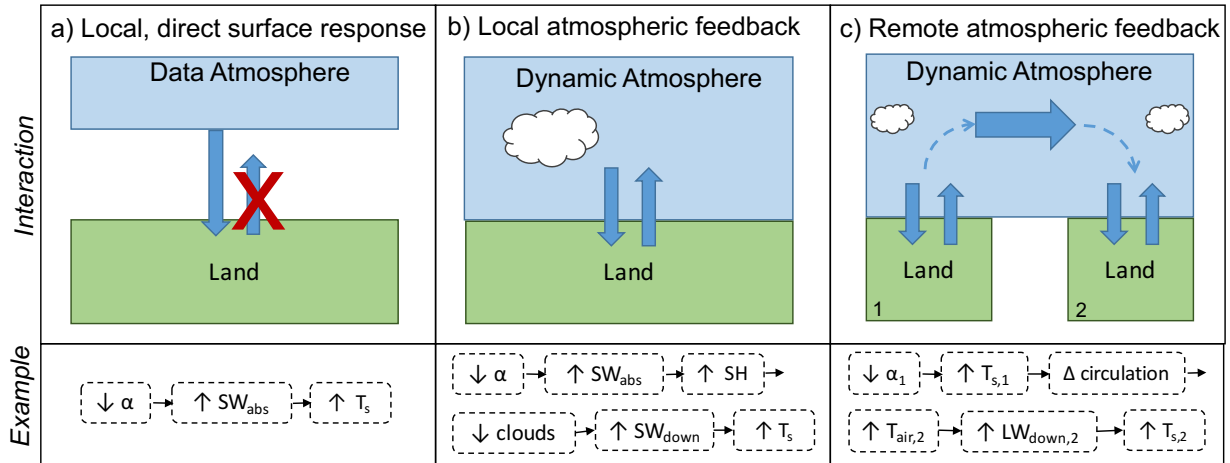
- 746 Neale, R. B., and Coauthors, 2012: Description of the NCAR community atmosphere model
747 (CAM 5.0). *NCAR Tech. Note NCAR/TN-486+STR*.
- 748 Shukla, J., and Y. Mintz, 2013: Influence of Land-Surface Evapotranspiration on the Earth ' s
749 Climate. *Science*, **215 (4539)**, 1498–1501, doi:10.1126/science.215.4539.1498.
- 750 Sud, Y. C., J. Shukla, and Y. Mintz, 1988: Influence of Land Surface Roughness on At-
751 mospheric Circulation and Precipitation: A Sensitivity Study with a General Circulation
752 Model. URL [http://journals.ametsoc.org/doi/abs/10.1175/1520-0450\(1988\)027%3C1036:](http://journals.ametsoc.org/doi/abs/10.1175/1520-0450(1988)027%3C1036:IOLSRO%3E2.0.CO;2)
753 [IOLSRO%3E2.0.CO;2%5Cn\(null\)](http://journals.ametsoc.org/doi/abs/10.1175/1520-0450(1988)027%3C1036:IOLSRO%3E2.0.CO;2), 1036–1054 pp., doi:10.1175/1520-0450(1988)
754 027%3C1036:IOLSRO%3E2.0.CO;2.
- 755 Swann, A. L. S., I. Y. Fung, and J. C. H. Chiang, 2012: Mid-latitude afforestation shifts general
756 circulation and tropical precipitation. *Proceedings of the National Academy of Sciences*, **109 (3)**,
757 712–716, doi:10.1073/pnas.1116706108.
- 758 Swann, A. L. S., I. Y. Fung, S. Levis, G. B. Bonan, and S. C. Doney, 2010: Changes in Arctic
759 vegetation amplify high-latitude warming through the greenhouse effect. *Proceedings of the*
760 *National Academy of Sciences*, **107 (4)**, 1295–1300, doi:10.1073/pnas.0913846107, URL [http:](http://www.pnas.org/cgi/doi/10.1073/pnas.0913846107)
761 [//www.pnas.org/cgi/doi/10.1073/pnas.0913846107](http://www.pnas.org/cgi/doi/10.1073/pnas.0913846107).
- 762 Swann, A. L. S., and Coauthors, 2018: Continental-scale consequences of tree die-offs in North
763 America: Identifying where forest loss matters most. *Environmental Research Letters*, **13 (5)**,
764 55 014, doi:10.1088/1748-9326/aaba0f.

LIST OF FIGURES

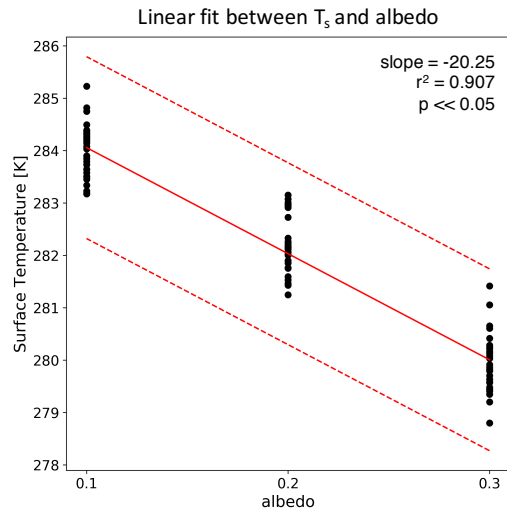
765
766
767
768
769
770
771
772
773
774
775
776
777
778
779
780
781
782
783
784
785
786
787
788
789
790
791
792
793
794
795
796
797
798
799
800
801
802
803
804
805
806
807
808

- Fig. 1.** Three types of land atmosphere interactions: (a) the direct, local response of the surface to the atmosphere (with no feedbacks); (b) local atmospheric feedbacks, where changes in the atmosphere above a modified land surface occur because of the modified land surface below that atmospheric column; (c) remote atmospheric feedbacks, where a change in land at location 1 drives a large-scale atmospheric response which can in turn impact the land at location 2. Examples of each feedback consider the impact of a change in albedo α on absorbed shortwave energy SW_{abs} , sensible heat flux SH , cloud cover, downwards shortwave energy at the surface SW_{down} , downwards longwave energy at the surface LW_{down} , and surface temperature T_s 39
- Fig. 2.** Example of calculation of the slope $\frac{\partial atm}{\partial land}$ for the response of surface temperature to changing surface albedo at 102.5°W, 42°N. Individual black dots show the annual mean temperature for a single year (30 years per spun-up simulation) at each of the three albedo levels. The solid red line shows the slope of the response, while the dashed red lines show 1 standard error around the slope. 40
- Fig. 3.** Annual mean scaled surface temperature T_s response [K] for (a-c) coupled simulations and (d-f) offline simulations, per 0.04 darkening of the surface albedo (a,d), 50 s/m increase in evaporative resistance (b,e), and 5.0 m decrease in vegetation height (c,f). Violet regions ($\Delta T_s < 0.1$) indicate regions where the temperature cooled substantially in response to the prescribed surface change. Stippling indicates regions where the slope is not significantly different from zero ($p > 0.05$). 41
- Fig. 4.** Annual mean change in surface energy fluxes [W/m²] per 0.04 decrease in global land albedo. Fluxes from the coupled simulations (a-d) are shown on the left, while offline fluxes (e-h) are shown on the right. Fluxes shown are net shortwave radiation (a,e), net longwave radiation (b,f), sensible heat flux (c,g), and latent heat flux (d,h). Red (blue) indicates an increase (decrease) in net shortwave radiation, net longwave radiation, and sensible heat flux. Blue (red) indicates an increase (decrease) in latent heat flux. Stippling indicates regions where the response is not significant ($p > 0.05$). 42
- Fig. 5.** Annual mean change in surface energy fluxes [W/m²] per 50 s/m increase in evaporative resistance. Fluxes from the coupled simulations (a-d) are shown on the left, while offline fluxes (e-h) are shown on the right. Fluxes shown are net shortwave radiation (a,e), net longwave radiation (b,f), sensible heat flux (c,g), and latent heat flux (d,h). Red (blue) indicates an increase (decrease) in net shortwave radiation, net longwave radiation, and sensible heat flux. Blue (red) indicates an increase (decrease) in latent heat flux. Stippling indicates regions where the response is not significant ($p > 0.05$) 43
- Fig. 6.** Annual mean change in surface energy fluxes [W/m²] per 5.0 m decrease in vegetation height. Fluxes from the coupled simulations (a-d) are shown on the left, while offline fluxes (e-h) are shown on the right. Fluxes shown are net shortwave radiation (a,e), net longwave radiation (b,f), sensible heat flux (c,g), and latent heat flux (d,h). Red (blue) indicates an increase (decrease) in net shortwave radiation, net longwave radiation, and sensible heat flux. Blue (red) indicates an increase (decrease) in latent heat flux. Stippling indicates regions where the response is not significant ($p > 0.05$) 44
- Fig. 7.** Difference in surface temperature response in coupled - offline simulations for (a) albedo, (b) evaporative resistance, and (c) vegetation height. 45

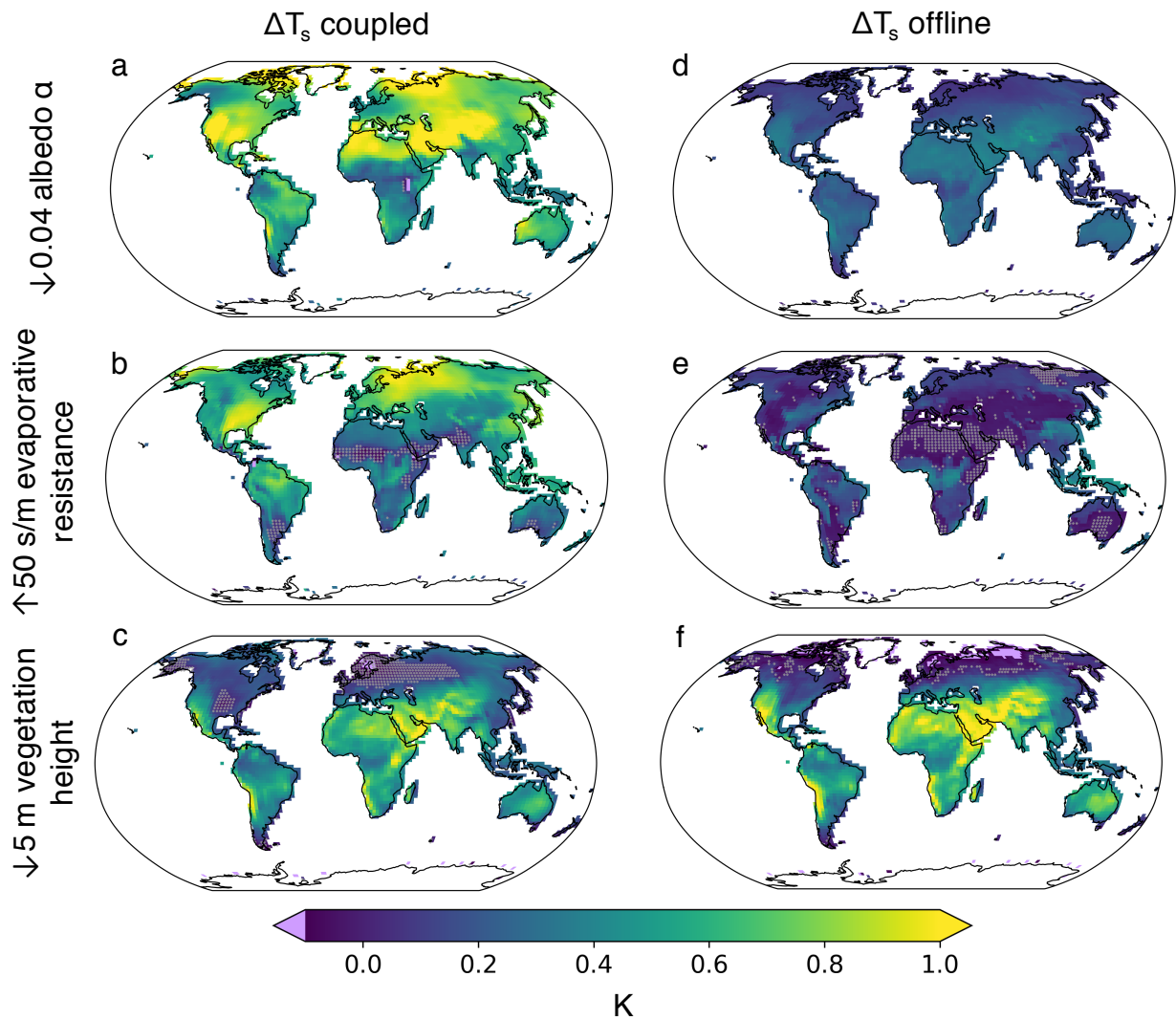
809	Fig. 8. Atmospheric feedback strength (percent change) for (a) albedo, (b) evaporative resistance,	
810	and (c) vegetation height.	46
811	Fig. 9. Change in (a) northward energy transport [Petawatts] and (b) zonal mean precipitation	
812	[mm/day] per 0.04 decrease in albedo (green), 50 s/m increase in evaporative resistance	
813	(blue), and 5 m decrease in vegetation height (orange).	47
814	Fig. 10. Change in surface property required to drive an 0.1 K warming in offline (left) and coupled	
815	(right) model simulations, for albedo (top), evaporative resistance (middle), and vegetation	
816	height (bottom).	48
817	Fig. 11. Change in surface temperature (left) and 2m air temperature (right) [K] per 0.04 decrease in	
818	land surface albedo (a,d), 50 s/m increase in land surface evaporative resistance (b,e), and	
819	5m decrease in land surface vegetation height . Stippling indicates regions which are not	
820	significant ($p < 0.05$), while light blue shows areas where the temperature response is less	
821	than -0.1 K.	49



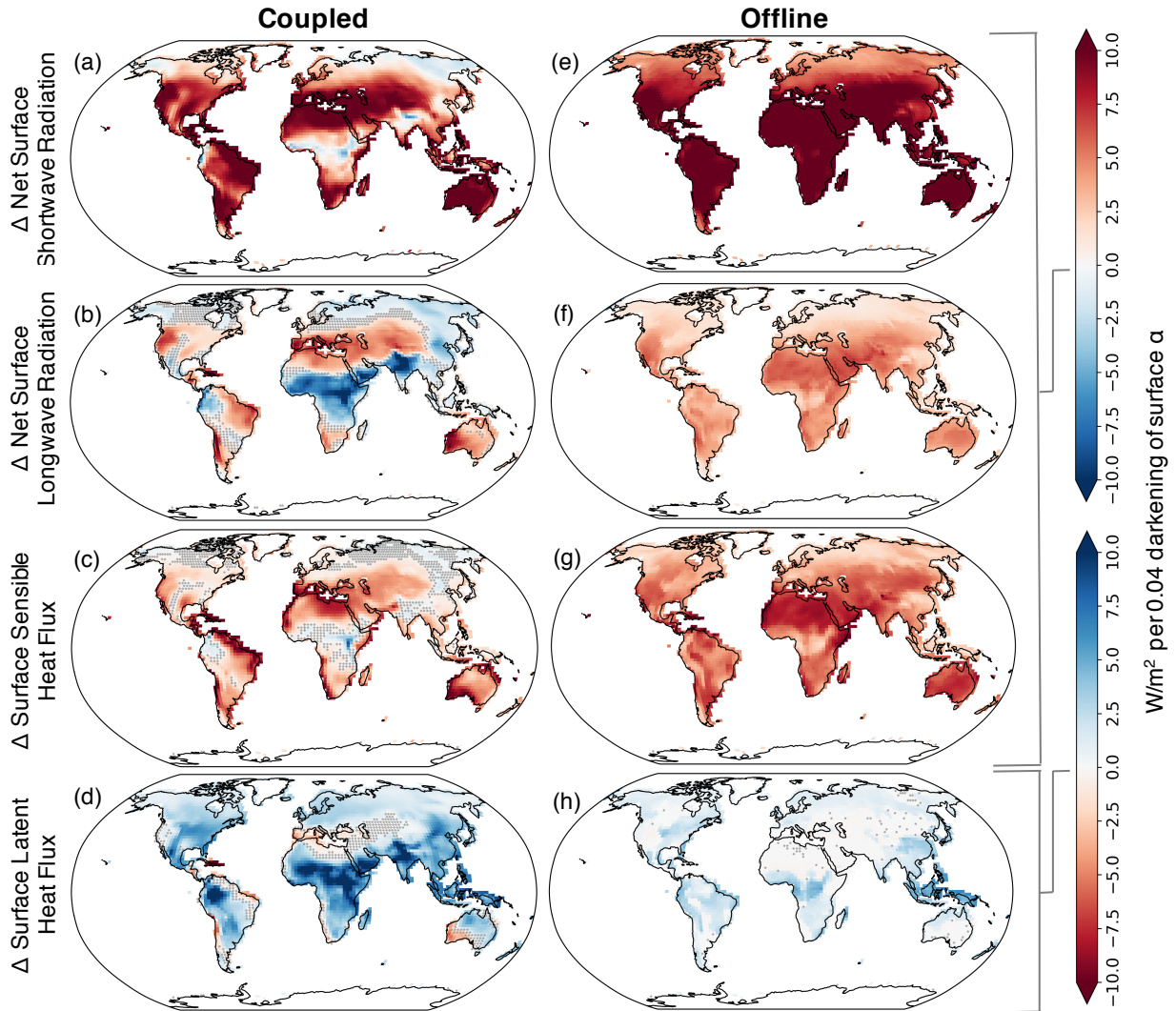
822 FIG. 1. Three types of land atmosphere interactions: (a) the direct, local response of the surface to the
823 atmosphere (with no feedbacks); (b) local atmospheric feedbacks, where changes in the atmosphere above a
824 modified land surface occur because of the modified land surface below that atmospheric column; (c) remote
825 atmospheric feedbacks, where a change in land at location 1 drives a large-scale atmospheric response which
826 can in turn impact the land at location 2. Examples of each feedback consider the impact of a change in albedo
827 α on absorbed shortwave energy SW_{abs} , sensible heat flux SH , cloud cover, downwards shortwave energy at the
828 surface SW_{down} , downwards longwave energy at the surface LW_{down} , and surface temperature T_s .



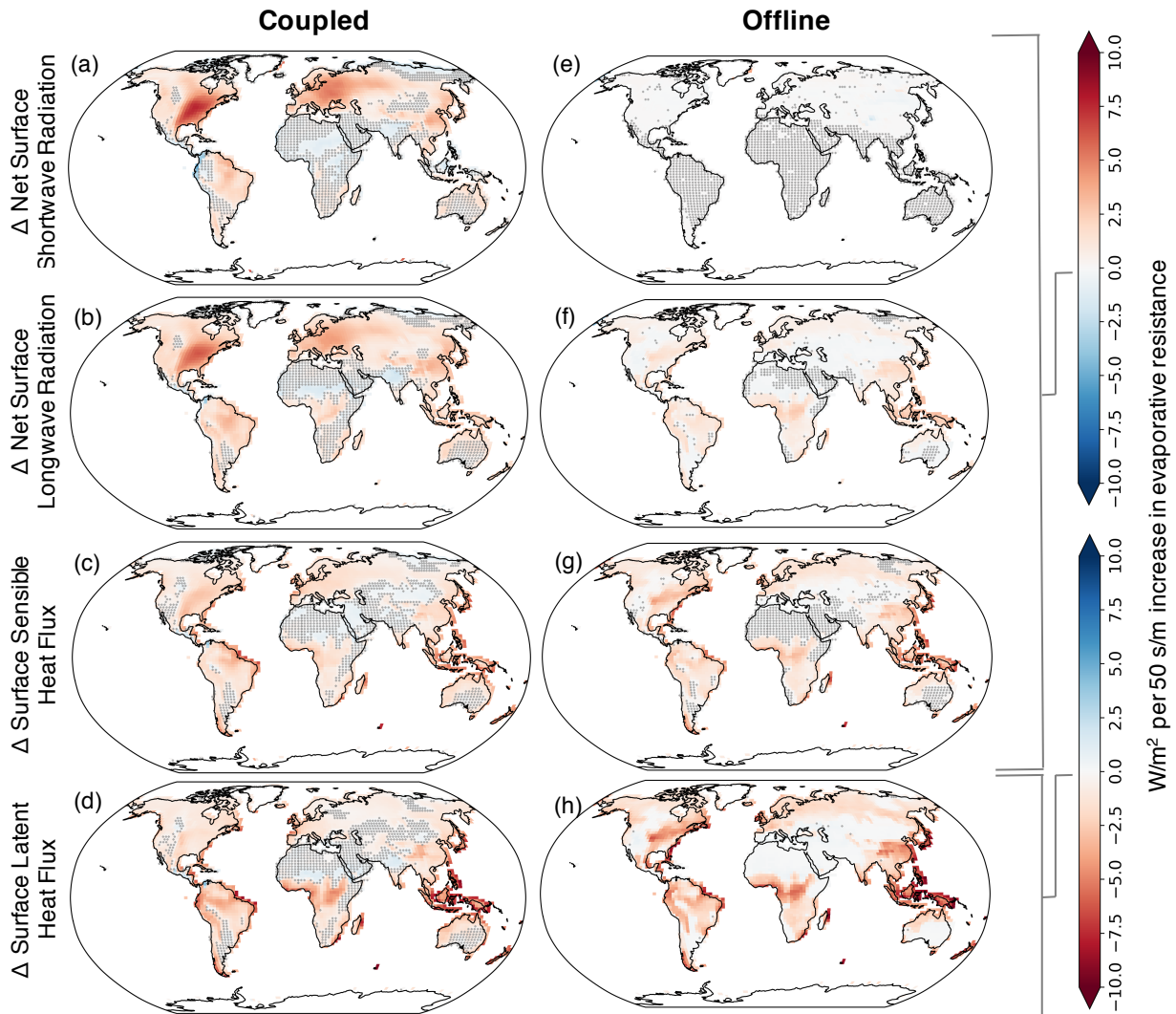
829 FIG. 2. Example of calculation of the slope $\frac{\partial T_s}{\partial \text{albedo}}$ for the response of surface temperature to changing surface
 830 albedo at 102.5°W, 42°N. Individual black dots show the annual mean temperature for a single year (30 years
 831 per spun-up simulation) at each of the three albedo levels. The solid red line shows the slope of the response,
 832 while the dashed red lines show 1 standard error around the slope.



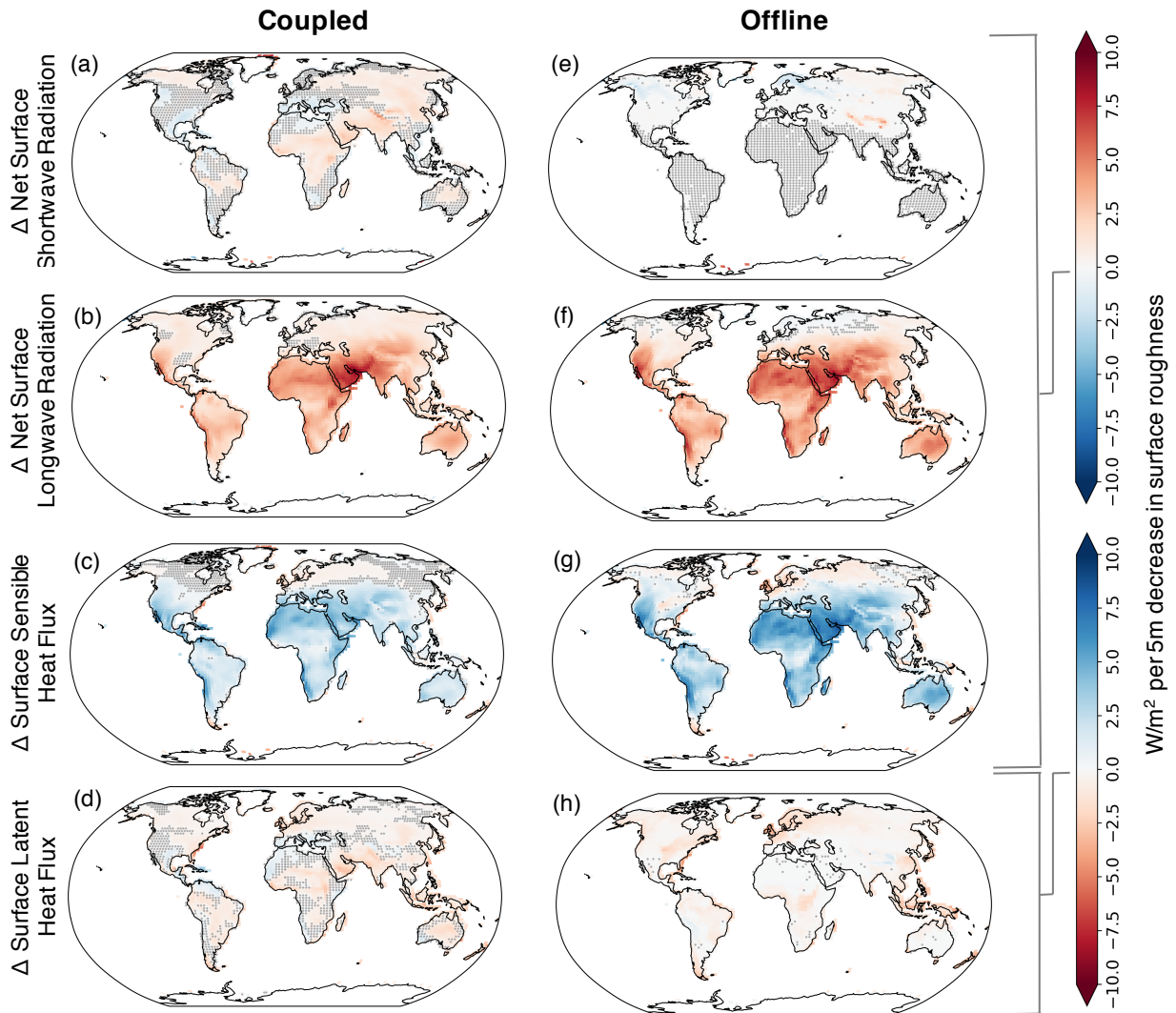
833 FIG. 3. Annual mean scaled surface temperature T_s response [K] for (a-c) coupled simulations and (d-f) offline
 834 simulations, per 0.04 darkening of the surface albedo (a,d), 50 s/m increase in evaporative resistance (b,e), and
 835 5.0 m decrease in vegetation height (c,f). Violet regions ($\Delta T_s < 0.1$) indicate regions where the temperature
 836 cooled substantially in response to the prescribed surface change. Stippling indicates regions where the slope is
 837 not significantly different from zero ($p > 0.05$).



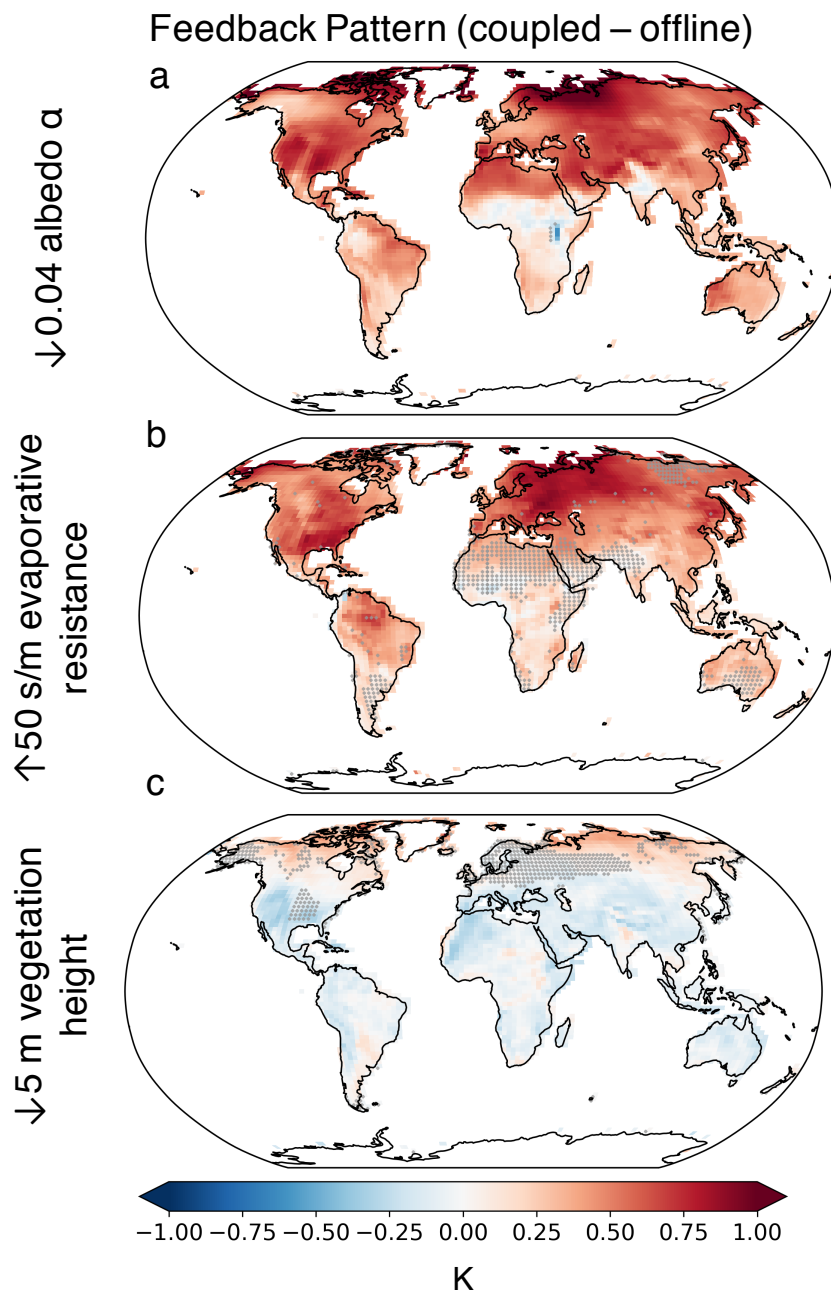
838 FIG. 4. Annual mean change in surface energy fluxes [W/m^2] per 0.04 decrease in global land albedo. Fluxes
 839 from the coupled simulations (a-d) are shown on the left, while offline fluxes (e-h) are shown on the right.
 840 Fluxes shown are net shortwave radiation (a,e), net longwave radiation (b,f), sensible heat flux (c,g), and latent
 841 heat flux (d,h). Red (blue) indicates an increase (decrease) in net shortwave radiation, net longwave radiation,
 842 and sensible heat flux. Blue (red) indicates an increase (decrease) in latent heat flux. Stippling indicates regions
 843 where the response is not significant ($p > 0.05$).



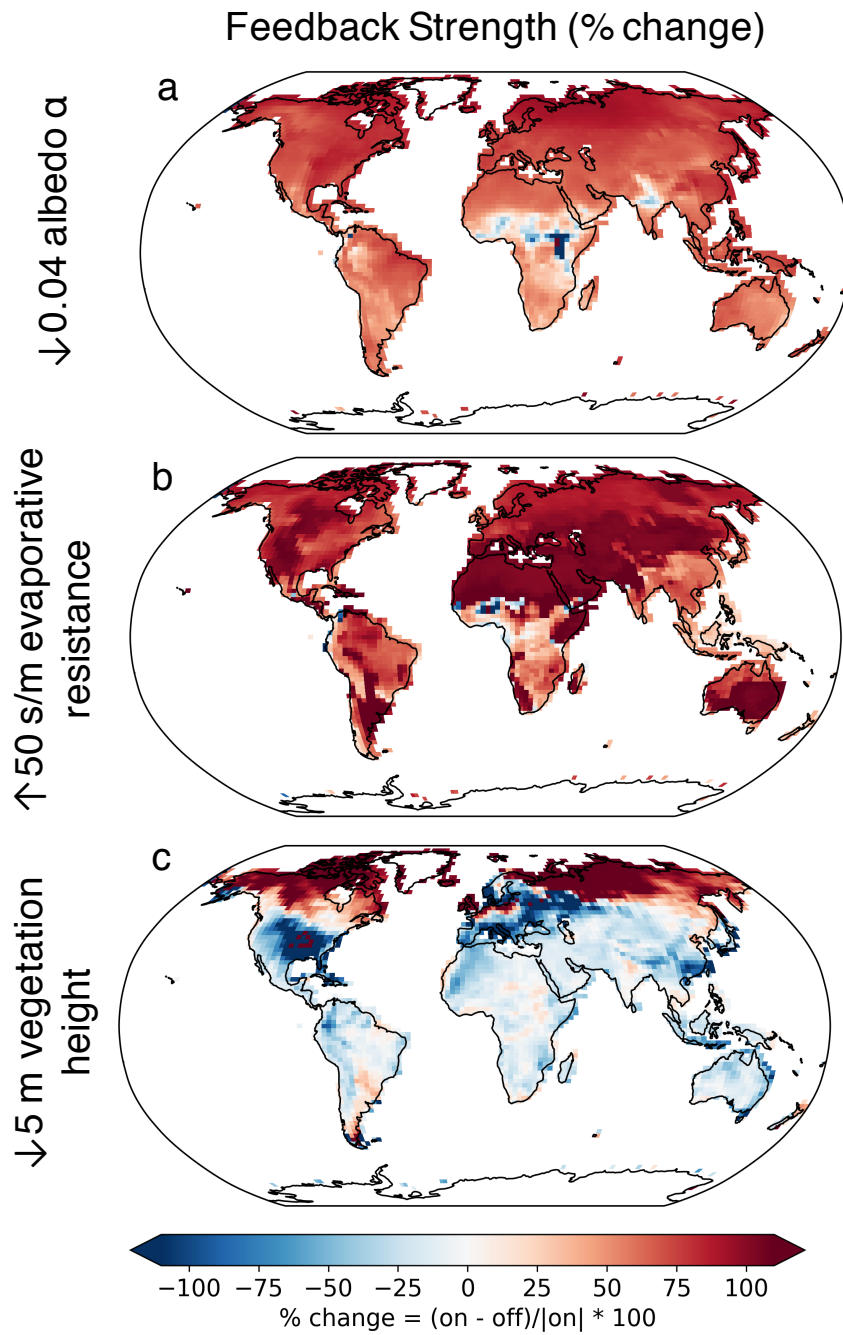
844 FIG. 5. Annual mean change in surface energy fluxes [W/m^2] per 50 s/m increase in evaporative resistance.
 845 Fluxes from the coupled simulations (a-d) are shown on the left, while offline fluxes (e-h) are shown on the right.
 846 Fluxes shown are net shortwave radiation (a,e), net longwave radiation (b,f), sensible heat flux (c,g), and latent
 847 heat flux (d,h). Red (blue) indicates an increase (decrease) in net shortwave radiation, net longwave radiation,
 848 and sensible heat flux. Blue (red) indicates an increase (decrease) in latent heat flux. Stippling indicates regions
 849 where the response is not significant ($p > 0.05$)



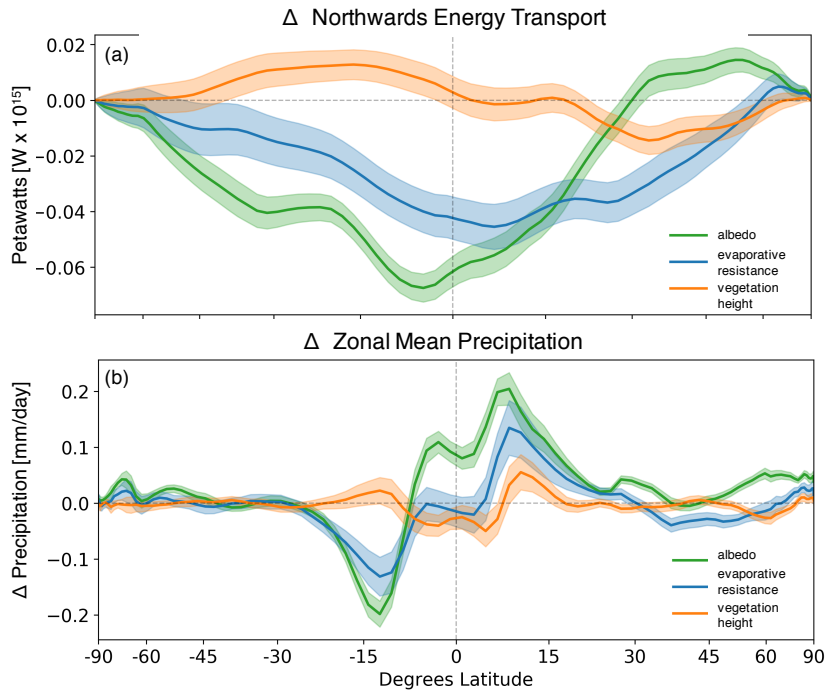
850 FIG. 6. Annual mean change in surface energy fluxes [W/m^2] per 5.0 m decrease in vegetation height. Fluxes
 851 from the coupled simulations (a-d) are shown on the left, while offline fluxes (e-h) are shown on the right.
 852 Fluxes shown are net shortwave radiation (a,e), net longwave radiation (b,f), sensible heat flux (c,g), and latent
 853 heat flux (d,h). Red (blue) indicates an increase (decrease) in net shortwave radiation, net longwave radiation,
 854 and sensible heat flux. Blue (red) indicates an increase (decrease) in latent heat flux. Stippling indicates regions
 855 where the response is not significant ($p > 0.05$)



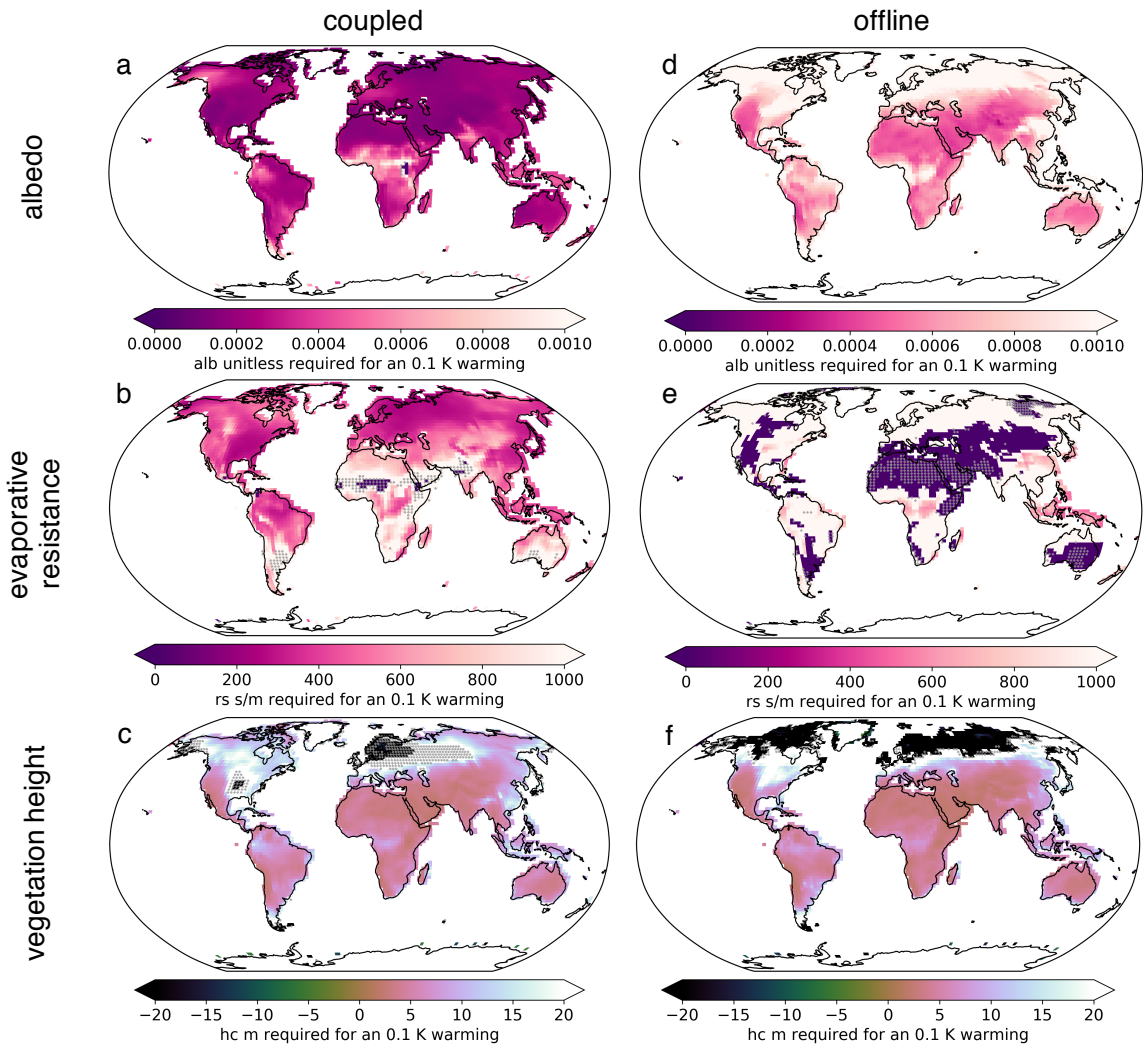
856 FIG. 7. Difference in surface temperature response in coupled - offline simulations for (a) albedo, (b) evapo-
 857 rative resistance, and (c) vegetation height.



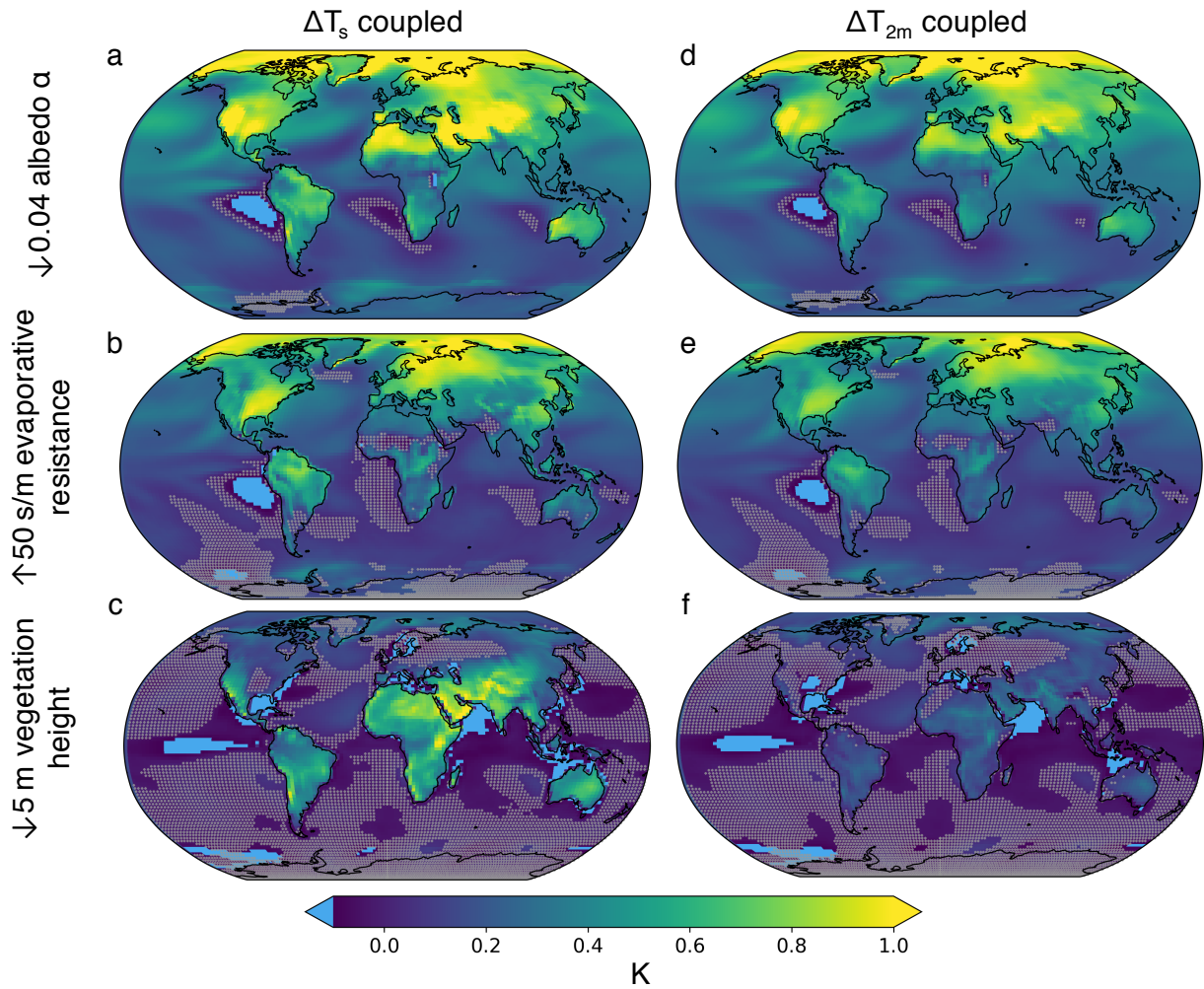
858 FIG. 8. Atmospheric feedback strength (percent change) for (a) albedo, (b) evaporative resistance, and (c)
 859 vegetation height.



860 FIG. 9. Change in (a) northward energy transport [Petawatts] and (b) zonal mean precipitation [mm/day] per
 861 0.04 decrease in albedo (green), 50 s/m increase in evaporative resistance (blue), and 5 m decrease in vegetation
 862 height (orange).



863 FIG. 10. Change in surface property required to drive an 0.1 K warming in offline (left) and coupled (right)
 864 model simulations, for albedo (top), evaporative resistance (middle), and vegetation height (bottom).



865 FIG. 11. Change in surface temperature (left) and 2m air temperature (right) [K] per 0.04 decrease in land
 866 surface albedo (a,d), 50 s/m increase in land surface evaporative resistance (b,e), and 5m decrease in land surface
 867 vegetation height . Stippling indicates regions which are not significant ($p < 0.05$), while light blue shows areas
 868 where the temperature response is less than -0.1 K.

Supplemental Material for

“The impact of individual land surface properties on terrestrial climate and atmospheric feedbacks”

Marysa Laguë, Abigail L. S. Swann, Gordon B. Bonan

December 8, 2018

This article is a non-reviewed preprint published at EarthArXiv

NOTICE:

From the AMS Copyright Policy section 7:

This work has not yet been peer-reviewed and is provided by the contributing author(s) as a means to ensure timely dissemination of scholarly and technical work on a noncommercial basis. Copyright and all rights therein are maintained by the author(s) or by other copyright owners. It is understood that all persons copying this information will adhere to the terms and constraints invoked by each author’s copyright. This work may not be reposted without explicit permission of the copyright owner. This work has been submitted to the *Journal of Climate*. Copyright in this work may be transferred without further notice. <https://www.ametsoc.org/index.cfm/ams/publications/ethical-guidelines-and-ams-policies/ams-copyright-policy/>

1 Simple Land Interface Model (SLIM) Model Description

1.1 Introduction

The Simple Land Interface Model (SLIM) is a simple land model written to couple with a global Earth System Model (ESM). In particular, this model is currently written to couple to the Commu-

nity Earth System Model (CESM [Hurrell et al., 2013]) in place of the Community Land Model (CLM [Lawrence et al., 2018]).

This simple model bears strong resemblance to some of the early global land surface models, and draws heavily from the parameterizations set forth in models including the land surface model of Manabe [1969]; the Biosphere Atmosphere Transfer Scheme (BATS) [Dickinson et al., 1993]; the Land Surface Model version 1 (LSM 1.0) [Bonan, 1996]; and the Land Dynamics Model (LaD) [Milly and Shmakin, 2002a], which was used as the LM2 land surface model in the GFDL AM2LM2 model [Anderson et al., 2004].

1.2 Land Surface Model

The simple land model solves a linearized bulk surface energy budget coupled with soil temperatures and bucket hydrology. Various physical properties determine how energy is partitioned within the surface energy budget (see table 1). Hydrology is represented with a simple “bucket”, which has a prescribed capacity. Additionally, there is a simple snow model which allows for land-albedo feedbacks during winter months.

1.2.1 Land Surface Properties

The land model has several properties which are defined by the user for each land point. These variables are listed in table 1. The variables are provided to the model using a netcdf file provided by the user, where each value is specified for every terrestrial gridpoint.

The surface albedo is prescribed for four different streams of radiation: visible direct, visible diffuse, near-infrared direct, and near-infrared diffuse, for both bare-ground (snow-free) and snow-covered ground. The emissivity ε of the ground can be specified. Land surface emissivities range from 0.9 to 1.0 [Bonan, 2002]; if unspecified, and for the purposes of this study, it is assumed that $\varepsilon = 1$ over all land areas.

In order to calculate temperature profiles within the 10 soil layers, the soil thermal conductivity κ and heat capacity c_v must be specified. Over glaciated regions (specified using a user-defined glacier mask), the thermal resistance and heat capacity of ice rather than soil are used. The bucket

model for hydrology requires a bucket capacity W_{max} (the maximum amount of water each gridcell can hold) and a surface “lid” resistance to evaporation r_s . The aerodynamic roughness is calculated from the vegetation height h_c . A simple snow model is included in SLIM; as snow accumulates on the land surface, it begins to mask the albedo of the snow-free surface such that the surface albedo approaches that of snow.

Prescribed Land Properties			
Variable	Typical Value	Units	Description
α_{gvd}	0.2	[unitless]	Visible direct albedo for bare ground.
α_{svd}	0.8	[unitless]	Visible direct albedo for deep snow.
α_{gnd}	0.3	[unitless]	Near-infrared direct albedo for bare ground.
α_{snd}	0.6	[unitless]	Near-infrared direct albedo for deep snow.
α_{gvf}	0.2	[unitless]	Visible diffuse albedo for bare ground.
α_{svf}	0.8	[unitless]	Visible diffuse albedo for deep snow.
α_{gnf}	0.3	[unitless]	Near-infrared diffuse albedo for bare ground.
α_{snf}	0.6	[unitless]	Near-infrared diffuse albedo for deep snow.
M_s	50	[kg/m ²]	Snow-masking depth: mass of water required in snow bucket to fully mask the bare ground albedo.
r_s	100	[s/m]	“Lid” resistance to evaporation
W_{max}	200	[kg/m ²] = [mm]	Bucket capacity: maximum amount of water the soil can hold
h_c	0.1-20.0	[m]	Vegetation height; used to calculate roughness lengths for momentum and heat.
$emissivity$	0.9-1.0	[unitless]	Surface emissivity for longwave radiation
glc_{mask}	logical	[unitless]	Mask marking gridcells which should be treated as glaciers/ice sheets.
$soil_{tk,1d}$	1.5	[W/m/K]	Thermal conductivity of soil (used for whole column).
$soil_{cv,1d}$	2.0e6	[J/m ³ /K]	Heat capacity of soil (used for whole column).
$glc_{tk,1d}$	2.4	[W/m/K]	Thermal conductivity of ice (used for whole column where glaciated).
$glc_{cv,1d}$	1.9e6	[J/m ³ /K]	Heat capacity of ice (used for whole column where glaciated).

Table 1: Typical values for each of the model parameters in SLIM.

1.2.2 Atmospheric Fluxes

At each time step the land model is run, information is required about the state of the atmosphere. This information can come either from a data atmosphere model (e.g. reanalysis), or from a coupled atmospheric model such as the Community Atmosphere Model [Neale et al., 2012]. The variables required from the atmosphere by the land model are given in table 2.

Variable	Information required from atmosphere	
	Units	Description
SW_{nd}^{\downarrow}	[W/m ²]	Direct, near-infrared incident solar radiation
SW_{vd}^{\downarrow}	[W/m ²]	Direct, visible incident solar radiation
SW_{ni}^{\downarrow}	[W/m ²]	Diffuse, near-infrared incident solar radiation
SW_{vi}^{\downarrow}	[W/m ²]	Diffuse, visible incident solar radiation
LW^{\downarrow}	[W/m ²]	Downwelling longwave radiation
z_{ref}	[m]	height of reference level for atmospheric variables given at reference height
T_{bot}	[K]	Temperature at lowest level of atmosphere
θ_{ref}	[K]	Potential temperature at reference height
q_{bot}	[kg/kg]	Specific humidity at lowest level of atmosphere
u_{ref}	[m/s]	Wind speed at reference height
e_{ref}	[Pa]	Vapor pressure at reference height
p_{bot}	[Pa]	Atmospheric pressure at lowest level of atmosphere
p_{surf}	[Pa]	Surface pressure
ρ_{air}	[kg/m ³]	Density of air at reference height
c_p	[J/kg/K]	Specific heat of air at constant pressure at reference height
$rain$	[m/s]	liquid precipitation
$snow$	[m/s]	frozen precipitation

Table 2: Table of values from the atmospheric model (or data atmosphere) required by the land model.

1.2.3 Surface Energy Budget

This model solves a linearized surface energy budget (eq 1) to calculate fluxes of energy and water to the atmosphere at each time step, and to calculate the surface temperature, temperature profile of the soil column, snow depth, and available water in each gridcell.

$$SW^\downarrow + LW^\downarrow = SW^\uparrow + LW^\uparrow + LH + SH + G \quad (1)$$

From the atmosphere, the land model receives the amount of downwards solar radiation SW^\downarrow for four radiation streams (visible direct, visible diffuse, near-infrared direct, and near-infrared diffuse), the amount of downwards longwave radiation LW^\downarrow , and information about the temperature, humidity, and wind speed of the bottom of the atmosphere. The land model calculates the reflected shortwave radiation SW^\uparrow , the upwards longwave radiation LW^\uparrow , the sensible heat flux SH , latent heat flux LH , and ground heat uptake G .

Equation 1 can be rewritten as

$$(1 - \alpha)SW^\downarrow + \varepsilon LW^\downarrow - LW^\uparrow = LH + SH + G$$

$$R_{in} = LW^\uparrow + LH + SH + G \quad (2)$$

$$R_{net} = LH + SH + G$$

where α is the albedo of the surface. $LW^\uparrow = \varepsilon\sigma T_s^4$ is the longwave radiation emitted by the surface, which is a function of surface temperature T_s and surface emissivity ε . R_{in} is the total absorbed radiative energy at the surface ($SW_{abs} + LW_{abs}$). R_{net} is the net radiative energy coming into the surface, which must be balanced by the turbulent energy fluxes (latent and sensible heat) and heat uptake by the land (soil or snow).

R_{in} can be directly calculated from the surface properties and atmospheric fluxes; $LW^\uparrow = \varepsilon\sigma T_s^4$, LH , SH , and G must each be found by evaluating the land model at each time step. In order to numerically calculate the balance of these fluxes at each time step, equation 2 is linearized around the change in surface temperature T_s .

That is, we calculate a ‘first guess’ at a flux (using the surface temperature from the previous time step), as well as the derivative of that flux with respect to surface temperature. We proceed to calculate a new surface temperature for the current time step, then update the surface fluxes given the initial estimate and its derivative with respect to temperature. This is equivalent to taking a

first order Taylor expansion of each surface flux (equation 4), where some flux F at time $i + 1$ is approximated by its value at time i and its derivative with respect to surface temperature T_s .

$$F(T_s^{i+1}) = F(T_s^i) + \frac{\delta F(T_s^i)}{\delta T_s}(T_s^{i+1} - T_s^i) + \mathcal{O}(T^2) \quad (3)$$

$$F(T_s^{i+1}) \approx F(T_s^i) + \frac{\delta F(T_s^i)}{\delta T_s}(T_s^{i+1} - T_s^i) \quad (4)$$

We solve the surface energy budget by linearizing each term with a first-order Taylor Expansion with derivatives w.r.t. surface temperature. i.e. for some surface flux S , its value at the $i + 1$ time step is its value at the i th time step plus its derivative w.r.t. temperature times the change in surface temperature:

$$S^{i+1} = S^i + \frac{\partial S}{\partial T_s} \Delta T_s. \quad (5)$$

For our longwave radiation, sensible heat flux, latent heat flux, and soil heat flux, this gives:

$$LW^{\uparrow i+1} = LW^{\uparrow i} + \frac{\partial LW^{\uparrow}}{\partial T_s} \Delta T_s \quad (6)$$

$$SH^{i+1} = SH^i + \frac{\partial SH}{\partial T_s} \Delta T_s \quad (7)$$

$$LH^{i+1} = LH^i + \frac{\partial LH}{\partial T_s} \Delta T_s \quad (8)$$

$$G^{i+1} = G^i + \frac{\partial G}{\partial T_s} \Delta T_s \quad (9)$$

$$R_{in}^{i+1} = (1 - \alpha)SW^{\downarrow i+1} - \varepsilon LW^{\downarrow i+1} \quad (10)$$

$$(11)$$

Thus, in order to calculate the surface fluxes for the $i + 1$ time step, we must first calculate the change in surface temperature ΔT_s , and the derivative of each flux with respect to temperature.

1.3 Radiative Fluxes

The longwave radiation LW^\uparrow [W/m^2] emitted from the surface, and its temperature derivative, are given by equations 12-13 as a function of the surface temperature at the preceding timestep T_s^i , where ε is the emissivity of the surface, and $\sigma = 5.670373 \times 10^{-8} \text{ W}/\text{m}^2/\text{K}^4$ is the Stefan-Boltzmann constant.

$$LW^\uparrow = \varepsilon\sigma(T_s^i)^4 \quad (12)$$

$$\frac{\delta LW^\uparrow}{\delta T_s} = 4\varepsilon\sigma(T_s^i)^3 \quad (13)$$

The absorbed downwards longwave radiation is a direct function of the downwelling longwave radiation LW^\downarrow and the surface emissivity ε . The absorbed shortwave radiation is a function of the downwelling shortwave radiation SW^\downarrow in each of the four radiation streams, and the surface albedo for each corresponding radiative stream. When a gridcell is free of snow, the bare-ground albedos are used. When there is snow on the ground (S , [kg/m^2]), a blend of the bare-ground and snow-covered albedos are used, following equation 14 (this is the default implementation of snow-covered ground albedo in Anderson et al. [2004], Milly and Shmakin [2002b]). A snow-masking factor M_s [kg] is used to define how steeply the bare-ground albedo should approach the snow-covered ground albedo (figure 1). A typical value of M_s used in SLIM is $50 \text{ kg}/\text{m}^2$, which corresponds to roughly 25cm of snow (assuming a snow density of $200 \text{ kg}/\text{m}^3$, typical of settled snow [Paterson, 1994]),

$$\alpha_j = \begin{cases} \alpha_{soil,j} & S = 0 \\ \left(1 - \frac{S}{S+M_s}\right)\alpha_{soil,j} + \frac{S}{S+M_s}\alpha_{snow,j} & 0 < S < M_s \\ \alpha_{snow,j} & S > M_s. \end{cases} \quad (14)$$

So, the total amount of incoming radiative energy from the atmosphere at each time step can

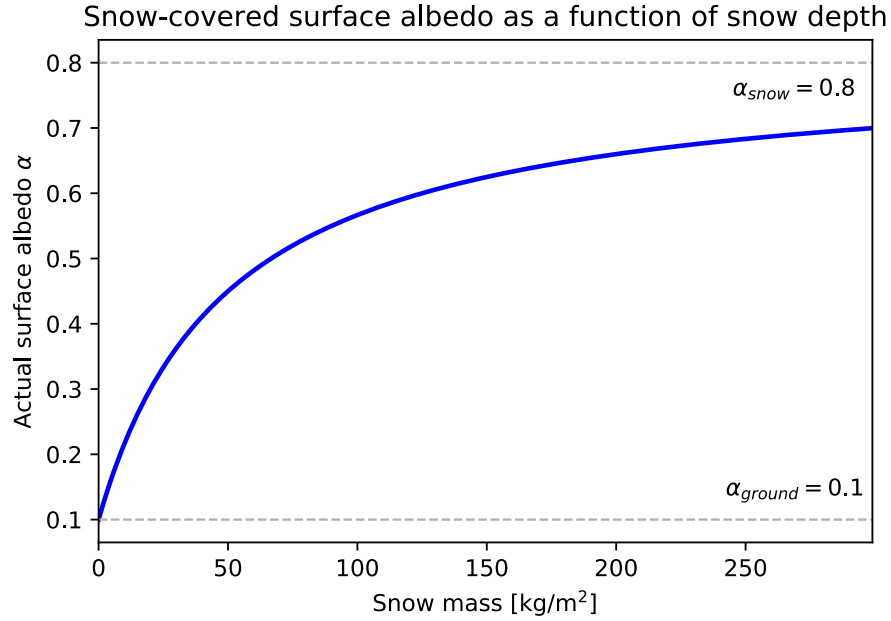


Figure 1: The albedo of a snow-covered gridcell as function of snow mass.

be directly calculated as

$$R_{in}^{i+1} = \sum_j (1 - \alpha_j) SW_j^{\downarrow i+1} + \varepsilon LW^{\downarrow i+1} \quad (15)$$

for the four shortwave radiative streams j .

1.4 Turbulent Heat Fluxes

The calculation of the turbulent heat fluxes (sensible and latent heat) relies on Monin-Obukhov theory [Monin and Obukhov, 1954]. Using the temperature, humidity, and wind speed of the bottom of the atmosphere, along with the temperature and humidity at the surface, the flux of heat and water can be calculated. These fluxes are influenced by the roughness of the land surface. The vegetation height h_c [m] provided by the surface property netcdf file is used to calculate a displacement height d (equation 16), a roughness length for momentum z_{0m} (equation 17), and a

roughness length for heat z_{0h} (equation 18).

$$d = 0.7h_c \quad (16)$$

$$z_{0m} = 0.1h_c \quad (17)$$

$$z_{0h} = 0.1z_{0m} \quad (18)$$

The above roughness lengths are used to calculate an Obukhov Length L , which in turn is used with the atmospheric temperature, humidity, and wind speed at the lowest atmospheric level to calculate an aerodynamic resistance for momentum r_{am} , heat r_{ah} , and moisture r_{aw} (in [s/m]). The Obukhov Length is calculated iteratively, with an initial estimate L_0 used to calculate the next estimate L_1 . In order to calculate the Obukhov Length, two intermediate functions ψ_m (for momentum) and ψ_h (for heat) are required (equations 20-21).

$$y = (1 - 16x)^{0.25} \quad (19)$$

$$\psi_m(x) = \begin{cases} 2 \log\left(\frac{1+y}{2}\right) + \log\left(\frac{1+y^2}{2}\right) - 2 \arctan(y) + \frac{\pi}{2} & \text{if } x < 0 \\ -5x & \text{if } x \geq 0 \end{cases} \quad (20)$$

$$\psi_h(x) = \begin{cases} 2 \log\left(\frac{1+y^2}{2}\right) & \text{if } x < 0 \\ -5x & \text{if } x \geq 0 \end{cases} \quad (21)$$

We use the reference level (typically 10m) atmospheric winds u_{ref} , temperature t_{ref} , and water vapour q_{ref} , the surface temperature t_s and water vapour q_s , as well as the dimensionless von Kármán constant $\kappa = 0.4$. Surface winds are assumed to be zero.

$$u^* = \frac{u_{ref}\kappa}{\log\left(\frac{z_{ref}-d}{z_{0m}}\right) - \psi_m\left(\frac{z_{ref}-d}{L_0}\right) + \psi_m\left(\frac{z_{0m}}{L_0}\right)} \quad (22)$$

$$t^* = \frac{(t_{ref} - t_s)\kappa}{\log\left(\frac{z_{ref}-d}{z_{0h}}\right) - \psi_h\left(\frac{z_{ref}-d}{L_0}\right) + \psi_h\left(\frac{z_{0h}}{L_0}\right)} \quad (23)$$

$$q^* = \frac{(q_{ref} - q_s)\kappa}{\log\left(\frac{z_{ref}-d}{z_{0h}}\right) - \psi_h\left(\frac{z_{ref}-d}{L_0}\right) + \psi_h\left(\frac{z_{0h}}{L_0}\right)} \quad (24)$$

$$t_v^* = t^* + 0.61t_s q^* \quad (25)$$

$$\theta_v = \theta_{ref}(1 + 0.61q_{ref}) \quad (26)$$

Equations 22-26 are then used to make a new estimate of the Obukhov length,

$$L_1 = \frac{u^{*2}\theta_v}{\kappa g t_v^*}. \quad (27)$$

Additionally, we limit the Obukhov Length to keep it within a range that gives reasonable flux values, in the following manner; this capping is common in land models [Anderson et al., 2004, Lawrence et al., 2018].

$$\zeta_0 = \frac{z_{ref} - d}{L_1} \quad (28)$$

$$\zeta = \begin{cases} \min(2, \zeta_0) & \text{if } \zeta_0 \geq 0 \\ \max(-2, \zeta_0) & \text{if } \zeta_0 < 0 \end{cases} \quad (29)$$

$$L_1 = \frac{z_{ref} - d}{\zeta} \quad (30)$$

The above equations are iterated over until the difference between L_0 and L_1 is small, up to a maximum of 40 iterations per time step. If the above fails to converge in 40 iterations, the value of L_1 with the smallest difference from its corresponding L_0 is used.

Using the final value of L_1 , final values of u^* and t^* are obtained, which are used to calculate the aerodynamic resistance of momentum r_{am} and heat r_{ah} (in units of [s/m]). We also calculate the aerodynamic resistance for moisture (r_{aw}), by combining the evaporative resistance for heat with the prescribed evaporative resistance r_s that the user directly controls (comparable to a bulk stomatal resistance for a canopy - this is how the user directly controls how difficult it is to evaporate water out of the bucket). The aerodynamic resistances require the use of several variables

from the atmospheric reference height z_{ref} (such as wind speed and air temperature):

$$r_{am} = \frac{u_{ref}}{u^* u^*} \quad (31)$$

$$r_{ah} = \frac{\theta_{ref} - T_s}{u^* T^*} \quad (32)$$

$$r_{aw} = r_s + r_{ah}. \quad (33)$$

The sensible heat flux SH [W/m²] is a function of the difference between the surface temperature T_s^i and the potential air temperature at the reference height θ_{ref}^i , as well as the roughness length for heat:

$$SH = c_{p,air} (T_s^i - \theta_{ref}^i) \frac{\rho_{air}}{r_{a,h}} \quad (34)$$

$$\frac{\delta SH}{\delta T_s} = c_{p,air} \frac{\rho_{air}}{r_{a,h}} \quad (35)$$

(where $c_{p,air}$ is the heat capacity of air and ρ_{air} is the density of air).

The latent heat flux LH [W/m²] is a function of the difference between the surface humidity and the humidity in the atmosphere. It is further impacted by the evaporative resistance r_s , the aerodynamic resistance r_{ah} , and another term, β , which accounts for bucket fullness (equation 36).

$$\beta = \min \left(\frac{water}{0.75 \times W_{max}}, 1.0 \right) \quad (36)$$

β is used to increase evaporative resistance under dry soil conditions. When the bucket is more than 75% full (ie the soil is moist), $\beta = 1$ (no additional resistance). When the bucket is less than 75% full, β decreases linearly from 1 to 0; the smaller the β term, the larger the resistance to evaporation.

The effective resistance of the land is a combination of the prescribed ‘‘lid’’ resistance r_s , the aerodynamic resistance due to the surface roughness r_{ah} (see equation 33), and the β value associ-

ated with how dry the soil is.

$$LH = \rho_{air} \lambda (q_s^i - q_{ref}^i) \frac{\beta}{r_{a,w}} \quad (37)$$

$$\frac{\delta LH}{\delta T_s} = \rho_{air} \lambda \frac{\delta q_s}{\delta T_s} \frac{\beta}{r_{a,w}} \quad (38)$$

In equation 38, ρ_{air} is the density of air, λ is the latent heat of vaporization (or sublimation, if temperatures are below freezing), q_s is the surface humidity, q_{ref} is the atmospheric humidity at some reference height, and T_s is the surface temperature. q_s , q_{ref} , and T_s are taken from the preceding time step i . Note that if the latent heat flux term attempts to evaporate (or sublimate) more water than is available in the combined water and snow buckets, the latent heat flux term is set to the total water plus snow available, and $\frac{\delta LH}{\delta T_s} = 0$, and the excess energy that would have been used by LH if more water were available is instead partitioned to SH.

1.4.1 Ground Heat Flux

The change in heat uptake by the soil $\frac{dG}{dT_s}$ requires solving the full temperature profile of the soil column. It is calculated using the energy imbalance of the other surface fluxes:

$$\begin{aligned} \frac{dG}{dT_s} &= \frac{\partial}{\partial T_s} (R_{in} - (LW^\uparrow + LH + SH)) \\ &= -\frac{\partial}{\partial T_s} LW^\uparrow - \frac{\partial}{\partial T_s} LH - \frac{\partial}{\partial T_s} SH, \end{aligned} \quad (39)$$

Heat transfer through the soil column is then calculated to get a new temperature for each soil layer, and a new surface temperature (section 1.4.3). Once the change in soil temperature at each soil layer (and specifically, the change in surface temperature T_s) is found, the total soil heat uptake G is given by

$$G^{i+1} = G^i + \frac{dG}{dT_s} (T_s^{i+1} - T_s^i), \quad (40)$$

where G^i is the energy flux into the soil at the previous time step i , $\frac{dG}{dT_s}$ is the derivative of the energy flux into the soil with respect to temperature. Here, G includes both the energy used to warm/cool the soil as well as any energy used to melt snow ($G = G_{soil} + G_{snow}$).

1.4.2 Hydrology

Water enters the land system by falling from the atmosphere as snow or rain. Water can fill up the bucket in each gridcell up to the bucket capacity W_{max} ; if the amount of water in a gridcell exceeds W_{max} , the excess is moved into runoff. At present, the runoff is discarded; if this model were run coupled to a dynamic ocean model, runoff water should be routed through an appropriate river-runoff scheme and added to the ocean model. Water is removed from the bucket either through runoff or evaporation (latent heat flux).

Snow can also fall onto grid cells. There is no limit on the amount of snow which can be held on a gridcell (note - this means snow accumulates indefinitely over the ice caps - a glacier calving scheme would need to be implemented to counteract this effect if it was undesirable for some application). The heat flux into the land G can be used to melt snow; melted snow flows into the water bucket.

1.4.3 Soil Temperatures

In order to solve equation 2, we must find ΔT_s . That is, we must calculate the new surface temperature. There are 10 soil layers in this model, with the midpoints of each soil layer given by equation 41:

$$z_i = -0.025 * (\exp(0.5 * (i - 0.5)) - 1.0) \quad i \in 1, 10. \quad (41)$$

The maximum soil depth is roughly 3.5m.

Soil temperatures are calculated using a simple heat diffusion equation through the soil layers, with a zero-flux bottom boundary condition (no energy can go in or out of the soil column through the bottom) and an upper boundary condition given by the G_{soil} term in the surface energy budget equation. Since the water in the bucket hydrology model is effectively isolated from the soil column, the amount of water in a given gridcell doesn't influence the soil thermal properties. Thus, in addition to the prescribed heat capacity and thermal conductivity of the soil, there is a fixed density of freezable water in each soil layer, which is not coupled to the amount of water actually present and available for evaporation in that gridcell. The soil *does* have a fixed density of

freezable water in each layer (set by default to 300 kg/m³). That is, the thin layers near the surface have a small amount of water in the soil layer which can be frozen/thawed using heat in that soil layer, while the deeper soil layers have a larger total volume of water available to freeze/thaw. This water is always present, and interacts with the soil **only** in a thermal manner. The water in the soil layers does not interact with the hydrology portion of the model - that is, it is not moved up and down between soil layers, and cannot be evaporated. The primary reason to include this freezable water in each soil layer is to allow the model to have a more realistic timescale of soil temperature change during spring and fall at high latitudes, where it takes time for the ground to freeze and thaw. This is comparable to the representation of water and soil in the LM2 model [Anderson et al., 2004].

We use the surface energy fluxes to update the soil temperature at each layer $n = 1 : N$ in the soil column, using the equation for heat diffusion:

$$c_{v,n} \frac{\partial T}{\partial t} = - \frac{\partial F}{\partial z}, \quad (42)$$

which can be re-arranged as

$$\partial T = - \frac{\Delta t}{c_{v,n} \Delta z_n} (F_{in} - F_{out}). \quad (43)$$

In eq 43, T is the temperature [K], Δt is the time step [s], $c_{v,n}$ is the heat capacity of the n^{th} layer [$J/m^3/K$], Δz_n is the thickness of soil layer n [m], and F_{in} and F_{out} are, respectively, the fluxes of energy into the top of and out of the bottom of the n^{th} soil layer [W/m^2].

At each soil layer, the fluxes into and out of each soil layer are given by:

$$F_n = \begin{cases} R_{in} - (LW^\uparrow + LH + SH) & n = 0 \text{ (top)} \\ -\kappa_{x,n} \frac{(T_n - T_{n+1})}{(z_n - z_{n+1})} & n = 1 : (N - 1) \\ 0 & n = N \text{ (zero-flux bottom)}. \end{cases} \quad (44)$$

where LW^\uparrow , LH , and SH are the linearized surface fluxes.

Representing each soil layer with the fluxes of energy into and out of that soil layer results in a tri-diagonal matrix which we solve using the Thomas Algorithm. We start at the bottom of the soil column and sweep up the matrix to solve for an initial estimate of surface temperature T_s . If there is no snow on the ground, or if there is snow on the ground, but T_s is below freezing, that T_s is used to complete the downwards sweep of the matrix and calculate the remaining soil temperatures. If the estimated surface temperature is above freezing and there is snow on the ground, the surface temperature is set to 0°C , and the difference between the predicted surface temperature and 0°C is used to melt snow. If there is still snow left after all the energy from the temperature difference is used, the surface temperature is kept at 0°C , and the downwards sweep of the matrix is used to calculate the temperature of the remaining soil layers. If there is enough energy associated with the difference in the predicted surface temperature and 0°C , all the snow is melted and the remaining energy is converted back to a temperature to calculate a modified T_s , which is then used to solve for the remaining soil temperatures. This representation of snow melt is comparable to that used in the LM2 model [Anderson et al., 2004]. The energy used to melt snow is saved as $G_{snow} = \text{snowmelt} \times h_{fus}$. A similar procedure is used to calculate the temperature profile of glaciated gridcells, but using the thermal properties of ice rather than soil.

After the soil temperatures have been calculated, we set the temperature of the top soil layer to be the surface temperature T_s (the topmost soil layer is very thin).

1.4.4 Water Accounting

Water enters the bucket via either rain (liquid precipitation) or snow melt. The bucket has a prescribed capacity; by default, the bucket capacity is 200 kg/m^2 (as in the LM2 code [Anderson et al., 2004]), but this can be modified to vary spatially by the user. Water can leave the bucket through evaporation (latent heat flux) or runoff (if the bucket exceeds capacity).

Snow accumulation is unlimited. Snow is added to the snow ‘bucket’ via snowfall (frozen precipitation) from the atmosphere. Snow can leave the snow bucket via either sublimation (directly to the atmosphere) or snow melt (to the water bucket on the land). Because snow accumulation is not limited by any ‘capacity’, this has the consequence that over glaciated regions, snow can

accumulate indefinitely. Because the land/atmosphere/slab-ocean system does not conserve water, this is not a problem (the atmosphere doesn't see any physical height to the snow), but if a dynamic ocean were used, a calving-scheme would need to be implemented to deposit ice into the ocean at high latitudes. This is similar to the implementation of snow in LM2 [Anderson et al., 2004].

1.5 Model behavior comparison with CLM

To demonstrate the general behavior of SLIM, we present a comparison of SLIM with CLM5 [Lawrence et al., 2018], forced with GSWP3 reanalysis data, repeating the data from year 2001-2010 for 50 years. Results shown are the average of the last 30 years of the simulations (allowing 20 years of model spin-up). CLM is run in bgc mode (interactive biogeochemistry) with an 1850 map of vegetation. The pattern of vegetation height for SLIM is derived from the last 30 years of the CLM5 simulation. The pattern of evaporative resistance is derived from the stomatal conductance, saved from the CLM5 simulation. The stomatal conductance in CLM5 is calculated separately for sunlit and shaded leaves; we weight the conductance by the leaf area of sunlit and shaded leaves then convert to units of resistance. The four streams of radiation impacted by surface albedo (visible/near-infrared direct/diffuse) are calculated from the summertime surface albedo of CLM5 (to avoid imposing any pattern of seasonal snow cover). Gridcells which have over 50% glacier cover in CLM5 are defined as glaciers in SLIM, and thus use the thermal properties of ice and albedo of snow.

Only summertime conductance and albedo values are used for each hemisphere (June, July, August in the Northern Hemisphere, and December, January, February in the Southern Hemisphere), but the resulting maps of surface conductance and albedo are fixed throughout the year in the SLIM simulations, while the CLM albedo can vary as leaf area and soil moisture change. Snow cover can modify this base-line albedo throughout the year in both SLIM and CLM5, but the snow-free albedo in the SLIM simulations has no seasonal cycle, nor does the evaporative resistance. The snow-masking depth is fixed to 50 kg/m² everywhere in this SLIM simulation (and is not a function of vegetation height, as it is in CLM).

As such, we do not expect SLIM to produce a surface climate identical to that of CLM; rather,

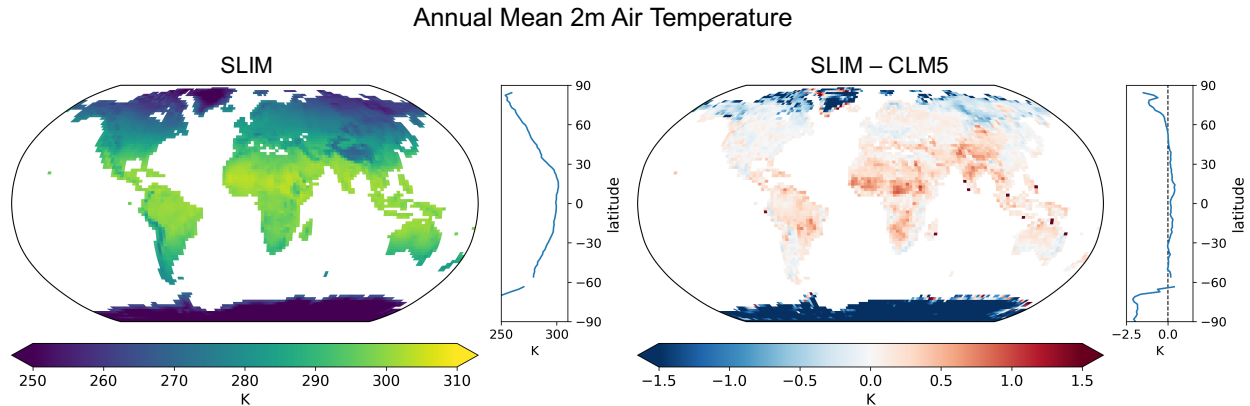


Figure 2: Annual mean 2m air temperature in the SLIM model (left), and the difference between SLIM and CLM5 (right). Both land models are forced with GSWP3 2001-2010 reanalysis.

we demonstrate that even with this fairly crude approximation of the vegetation patterns of CLM, SLIM can still produce surface temperatures and fluxes comparable to those from the much more complex CLM.

The annual mean temperature of SLIM is comparable to that of CLM in most regions (figure 2). Portions of the northern high latitudes are over 1K cooler in SLIM than CLM, largely due to SLIM having a much brighter snow albedo over non-glaciated regions. Over the interior of Antarctica, sensible heat fluxes are slightly (10 W/m^2) too high and longwave fluxes are too low (figure 3). Albedo differences along the Antarctic coast (non-glaciated regions, where albedo is calculated as a combination of ground albedo and snow) additionally contribute to differences in surface temperature and surface energy fluxes.

Parts of the tropics and mid-latitudes are too hot (notably the Sahara/Sahel region of Africa, and the Tibetan plateau; figure ??). Over the Tibetan plateau, SLIM has a lower albedo (is darker), contributing to the warmer surface temperatures (figure 4). Over the Sahara, sensible heat fluxes are too low (perhaps because of surface roughness differences) resulting in warmer surface temperatures. In sub-saharan Africa, indeed in most of the tropics, latent heat fluxes are much lower than in CLM, which are roughly compensated for by sensible heat fluxes which are higher than in CLM (figure 3). That is, with the maps of surface properties used in this simulation of SLIM, the evaporative fraction is much lower than that of CLM. Seasonal cycles are shown for four locations

Annual mean surface energy fluxes

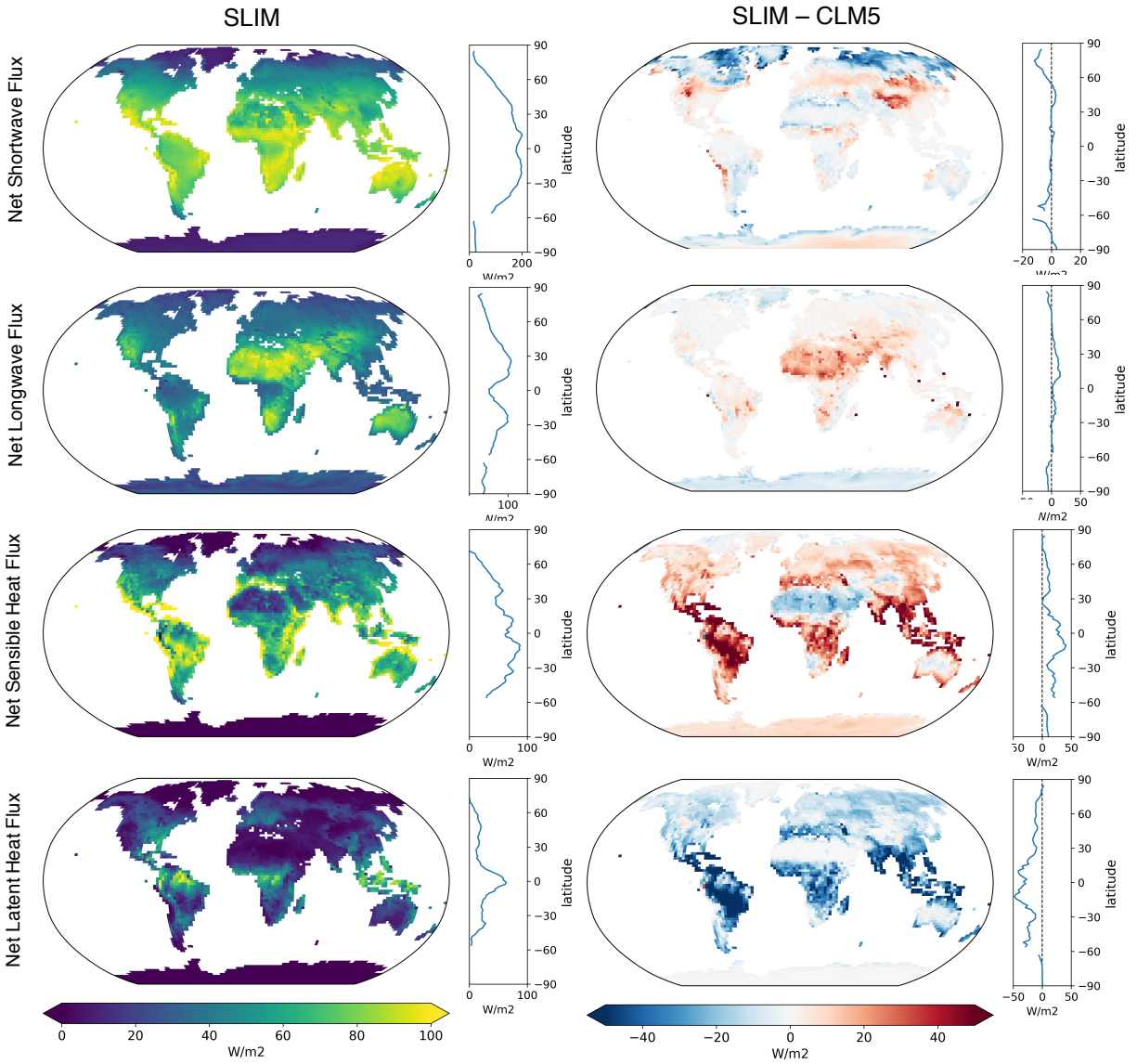


Figure 3: Annual mean surface energy budget: net flux of shortwave radiation (row 1), net flux of longwave radiation (row 2), sensible heat flux (row 3), and latent heat flux (row 4) for the SLIM model (left column), and the difference between SLIM and CLM5 (right column).

Annual mean land albedo

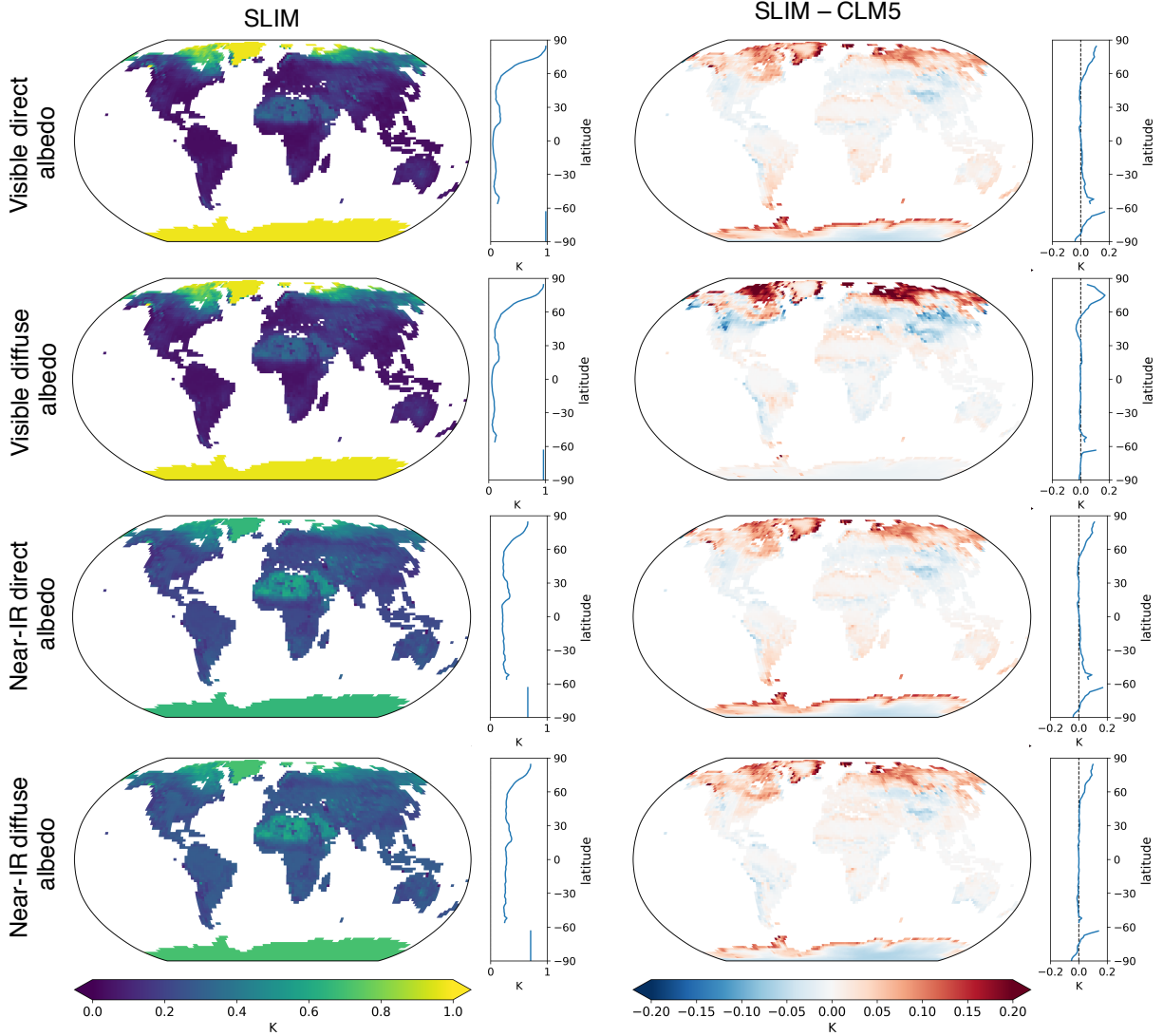


Figure 4: Annual mean land albedo for visible direct radiation (row 1), visible diffuse radiation (row 2), near-infrared direct radiation (row 3), and near-infrared diffuse radiation (row 4) for the SLIM model (left column), and the difference between SLIM and CLM5 (right column).

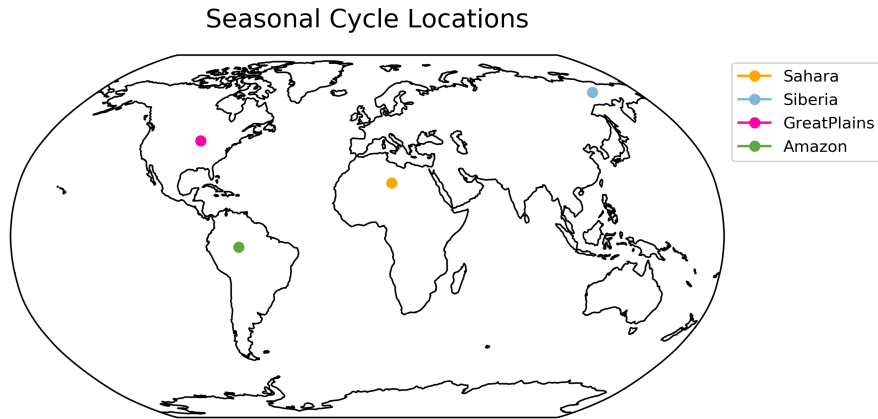


Figure 5: Locations used for seasonal cycle plots: Sahara: 23.7°N, 12.5°E (orange); Siberia: 65.4°N, 150°E (blue); Great Plains: 42.6°N, 92.5°W (pink); Amazon: 4.7°S, 65°W (green).

with very different climates: the Sahara, the Amazon, Siberia, and the Great Plains (figure 5). The seasonal cycle of temperature is very similar between SLIM and CLM (figure 6), as the seasonal temperature differences driven by the atmospheric forcing data are much larger than the difference in temperature produced by the land models themselves. The differences between SLIM and CLM in individual terms of the surface energy budget are much larger than the differences in temperature, mostly coming from a difference in evaporative fraction: when latent heat flux in SLIM is lower than in CLM, sensible heat flux tends to be higher (figure 7).

The seasonal cycle of soil temperatures is physically consistent with our intuition (figure 8). In all areas, the peak in surface soil temperatures occurs in summer, with the peak in deep soil temperatures lagging. Deep soils are cooler than surface soils in summer, and warmer than surface soils in winter, as we would expect, with the ground taking up heat during warm summer months and releasing heat during cold winter months. The soil properties of all non-glaciated land areas in SLIM are identical in this simulation. The diurnal temperature profile of soil temperatures is also consistent with our physical expectation, with surface soil temperatures having a large diurnal temperature cycle and deep soils having no diurnal temperature cycle, and surface soil temperatures peak a few hours after local noon (figure 9).

SLIM executes over 98% faster than CLM.

Climatological 2m Air Temperature in SLIM and CLM5

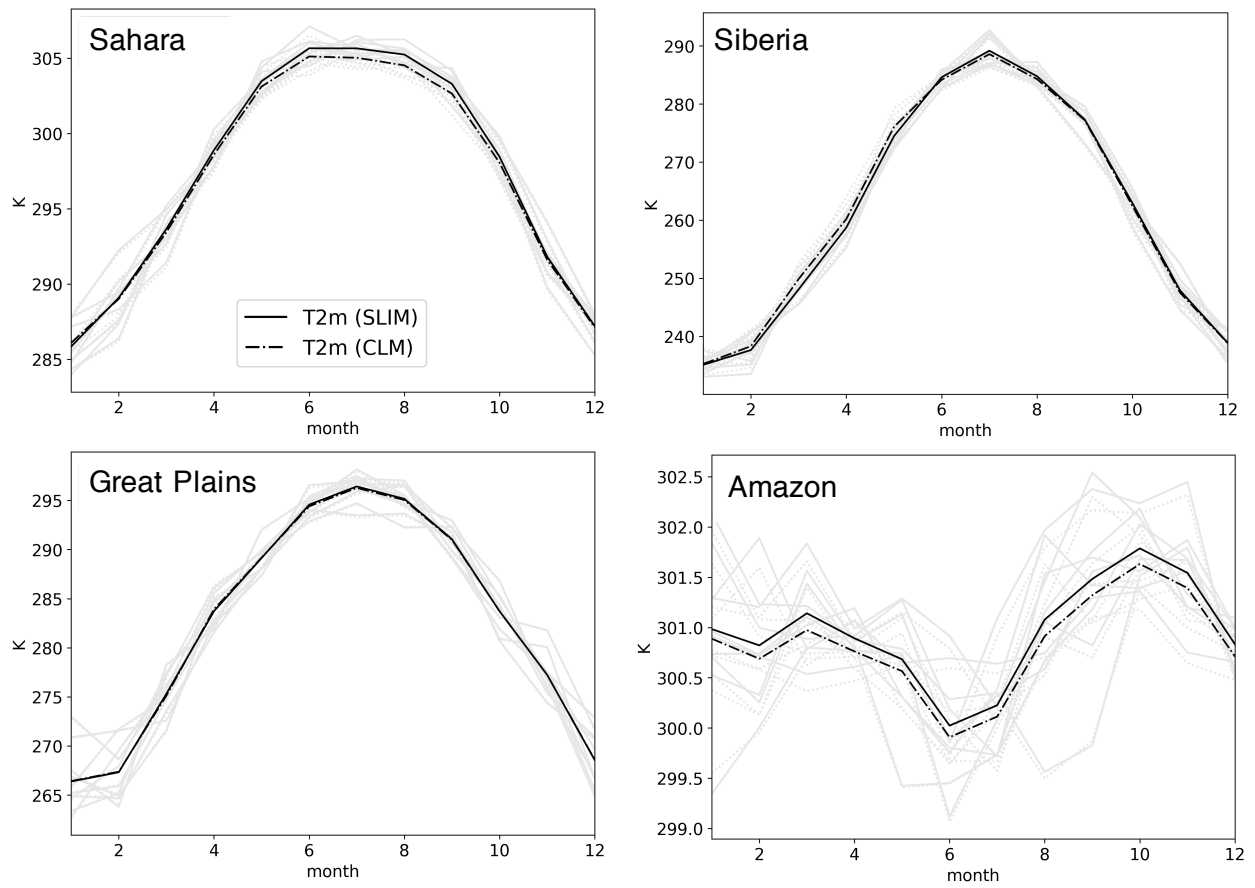


Figure 6: Seasonal cycle of 2m air temperature [K] over 4 locations in SLIM (solid lines) and CLM5 (dash-dot lines). The climatological cycle is shown in black lines, while individual years are shown in gray.

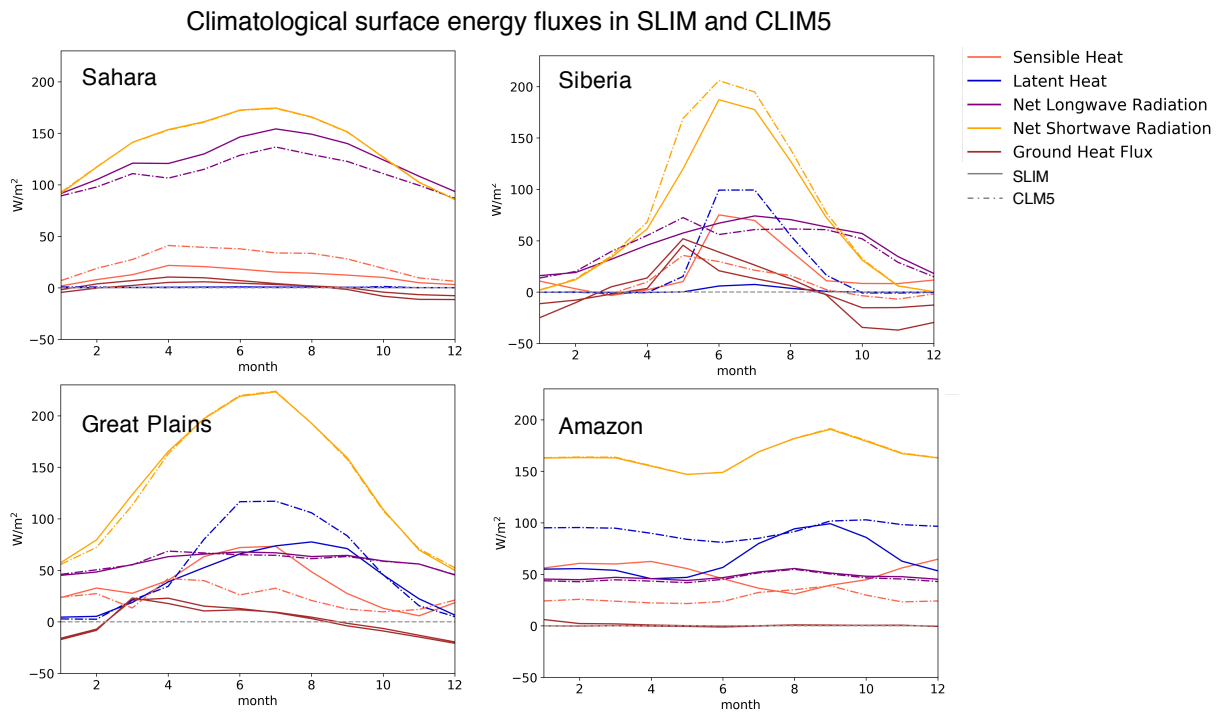


Figure 7: Seasonal cycle of the individual terms of the surface energy budget [W/m^2] over 4 locations in SLIM (solid lines) and CLM5 (dash-dot lines). The net flux of shortwave radiation (absorbed shortwave) is shown in yellow; net longwave radiation (positive upwards) is shown in purple; sensible heat (positive upwards) is shown in red; latent heat (positive upwards) is shown in blue; ground heat flux (heat uptake by soil or snow) is shown in brown.

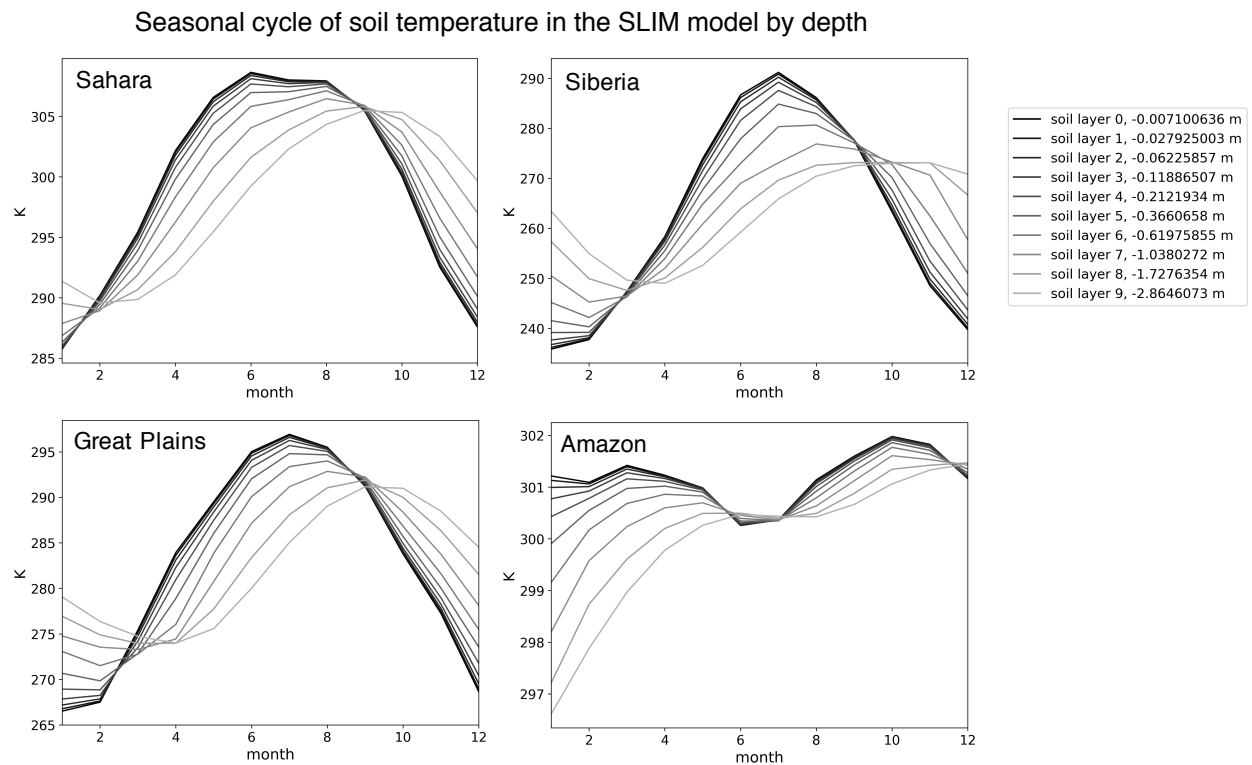


Figure 8: Seasonal cycle of soil temperature over 4 locations in SLIM, as a function of soil depth (darker lines are closer to the surface, lighter lines are deeper in the soil).

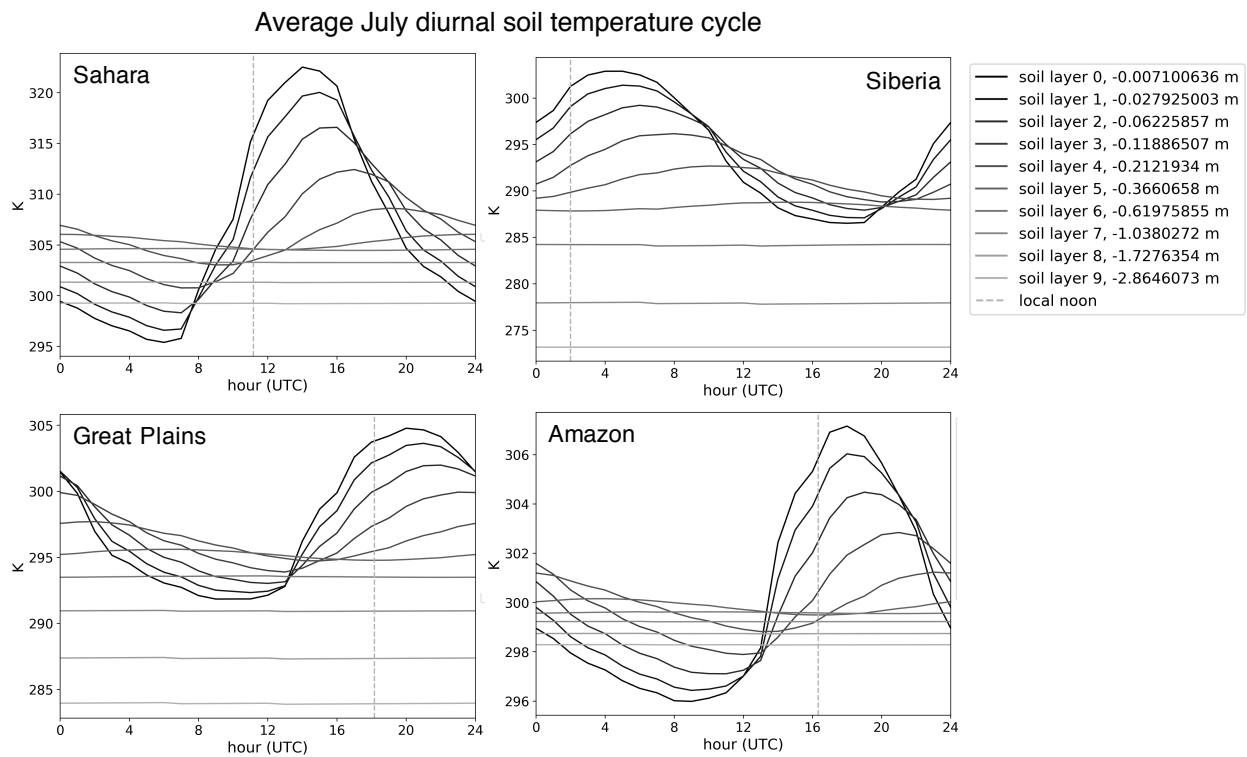


Figure 9: Diurnal cycle of soil temperature (averaged over all July days in a single year) over 4 locations in SLIM, as a function of soil depth (darker lines are closer to the surface, lighter lines are deeper in the soil). Local noon is indicated by the vertical dashed gray line.

2 Supplemental Figures

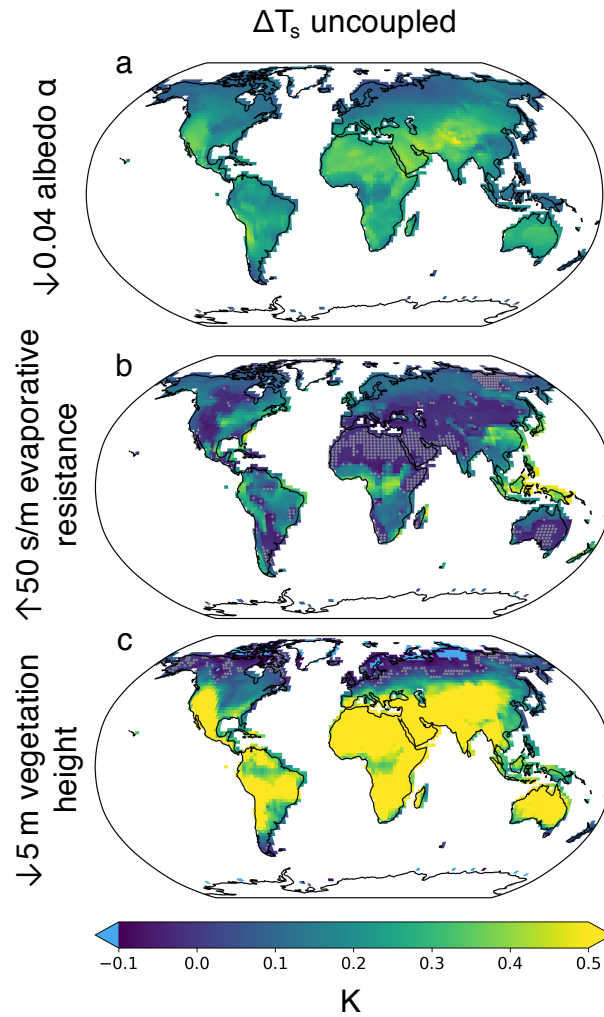


Figure 10: Surface temperature response to changing surface properties, but with a smaller range to better show spatial pattern of temperature response in offline simulations only. Annual mean scaled surface temperature T_s response [K] for the offline simulations, per 0.04 darkening of the surface albedo (a), 50 s/m increase in evaporative resistance (b), and 5.0 m decrease in vegetation height (c). Cyan regions ($\Delta T_s < 0.1$) indicate regions where the temperature cooled substantially in response to the prescribed surface change.

Downwelling Shortwave Radiation at Surface

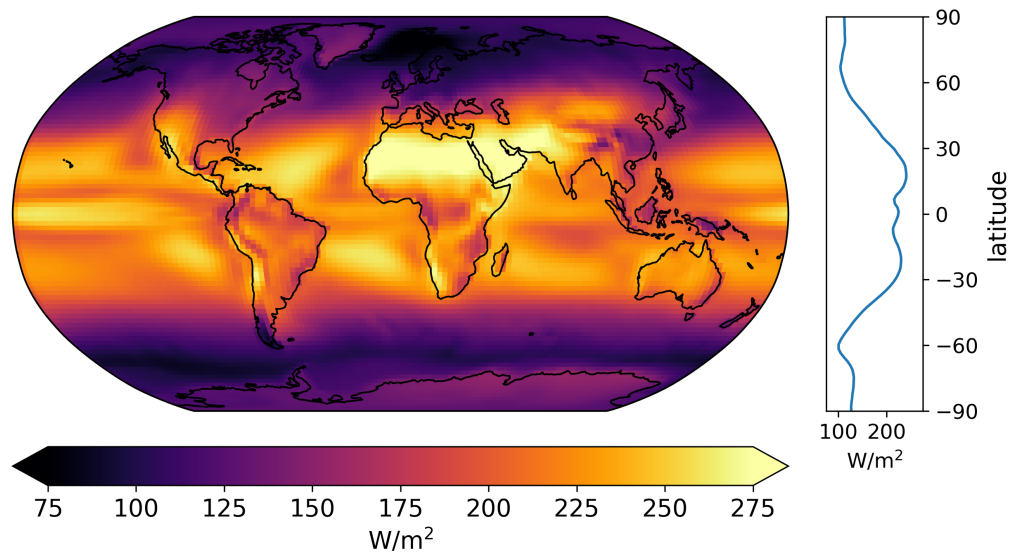


Figure 11: Annual mean downwelling shortwave radiation at the surface [W/m^2] in the ‘baseline’ simulation (albedo = 0.2, evaporative resistance = 50 s/m, vegetation height = 0.1 m).

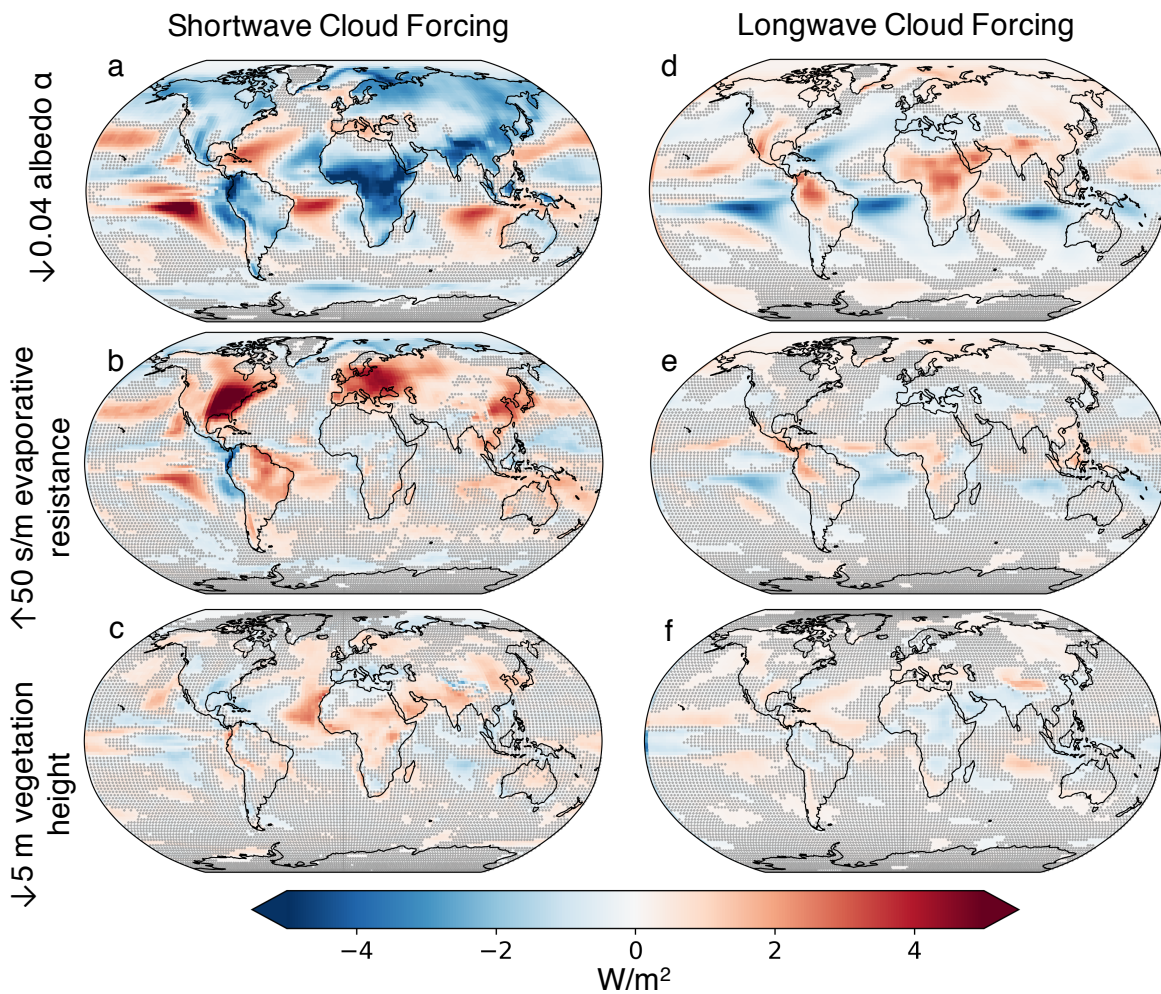


Figure 12: Change in shortwave cloud forcing (left) and longwave cloud forcing (right) per 0.04 decrease in albedo (a,d), 50 s/m increase in evaporative resistance (b,e), and 5 m decrease in vegetation height (c,f). Stippling indicates statistically insignificant regions ($p > 0.05$).

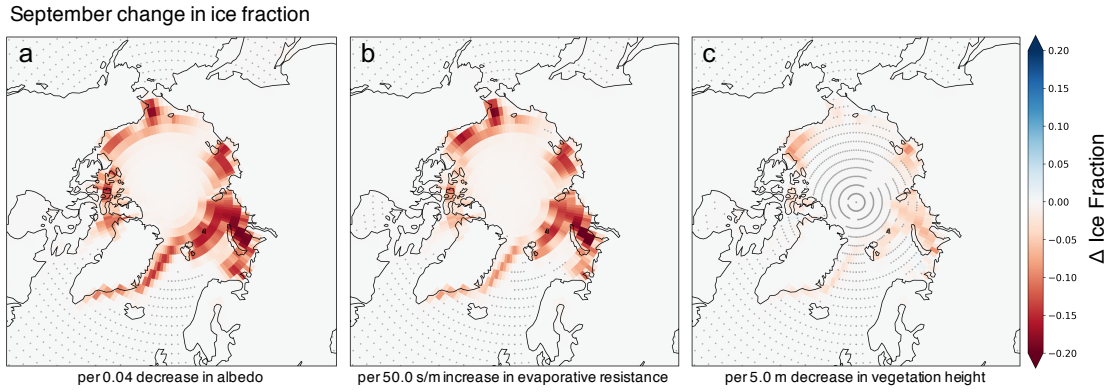


Figure 13: Change September ice fraction per (a) 0.04 decrease in land albedo, (b) 50 s/m increase in land surface evaporative resistance, and (c) 5m decrease in land surface vegetation height. Stippling indicates regions which are not significant ($p > 0.05$).

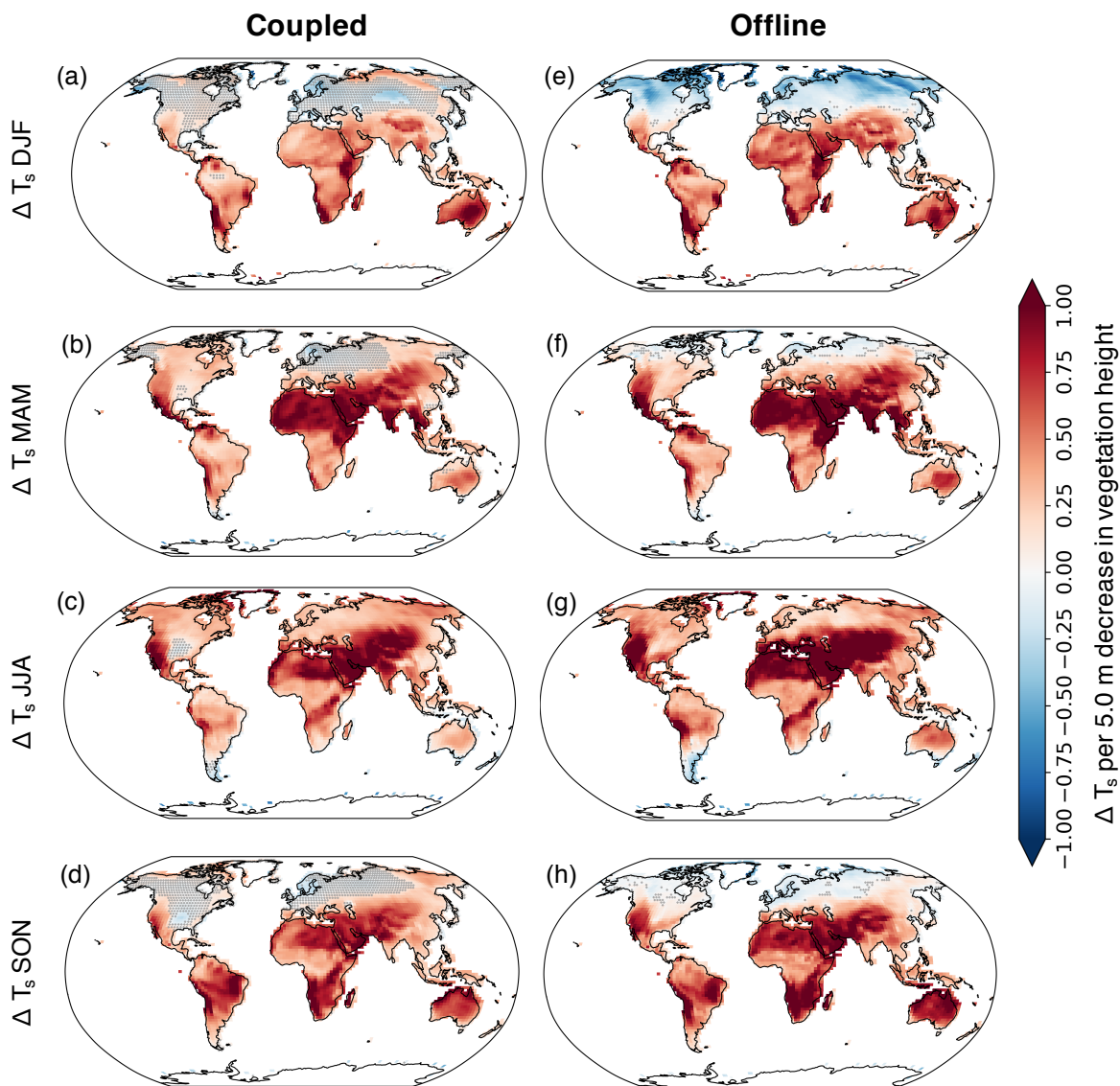


Figure 14: Seasonal change in surface temperature T_s per 5.0 m decrease in vegetation height in the coupled (left) and offline (right) simulations. Stippling indicates insignificant changes with $p < 0.05$.

Δ Annual Mean Cloud Fraction (albedo)

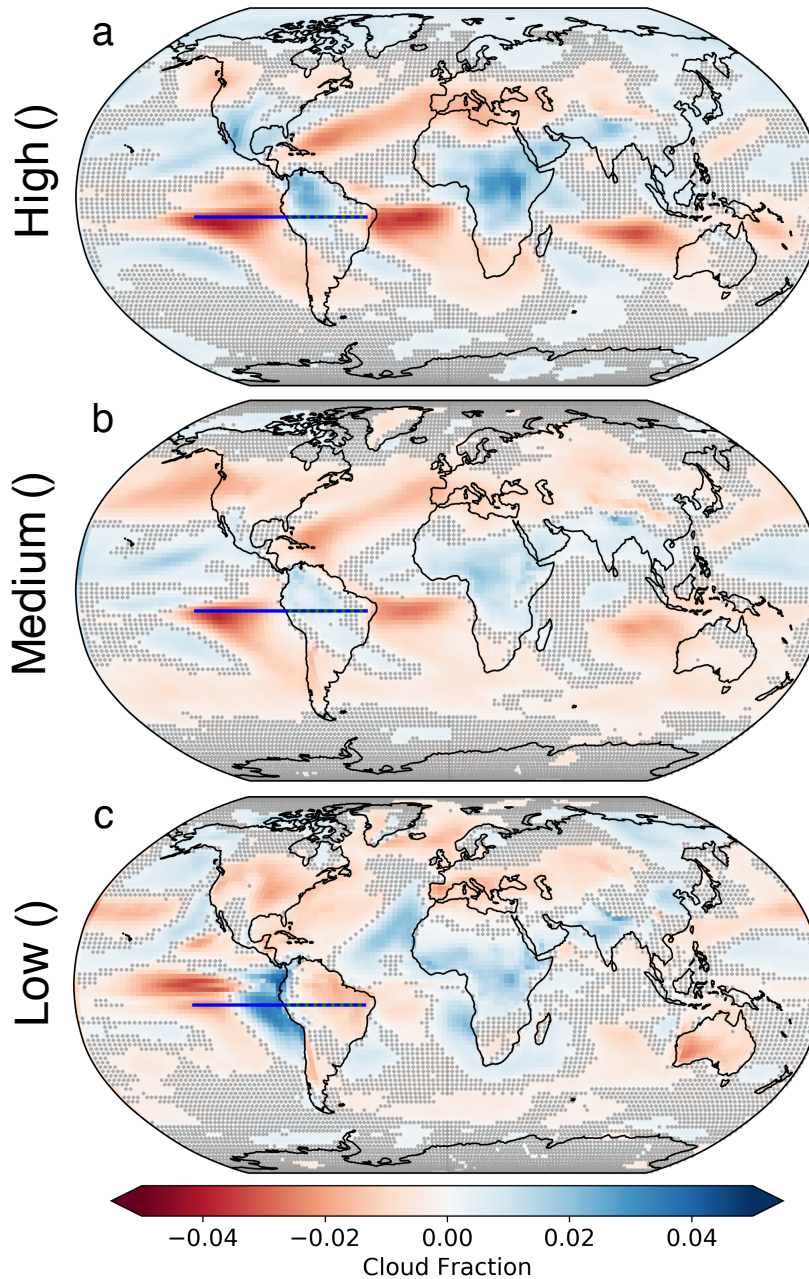


Figure 15: Annual mean change in cloud fraction per 0.04 decrease in surface albedo for (a) high (400 hpa - top of model), (b) medium (700-400 hpa) and (c) low (surface - 700 hpa) clouds per 0.4 decrease in surface albedo. Stippling indicates insignificant changes with $p > 0.05$. Horizontal blue lines show the region where subsidence was analyzed (not shown).

References

- Anderson, J. L., Balaji, V., Broccoli, A. J., Cooke, W. F., Delworth, T. L., Dixon, K. W., Donner, L. J., Dunne, K. a., Freidenreich, S. M., Garner, S. T., Gudgel, R. G., Gordon, C. T., Held, I. M., Hemler, R. S., Horowitz, L. W., Klein, S. a., Knutson, T. R., Kushner, P. J., Langenhost, A. R., Lau, N. C., Liang, Z., Malyshev, S. L., Milly, P. C. D., Nath, M. J., Ploshay, J. J., Ramaswamy, V., Schwarzkopf, M. D., Shevliakova, E., Sirutis, J. J., Soden, B. J., Stern, W. F., Thompson, L. a., Wilson, R. J., Wittenberg, A. T., Wyman, B. L., Anderson, J. L., Balaji, V., Broccoli, A. J., Cooke, W. F., Delworth, T. L., Dixon, K. W., Donner, L. J., Dunne, K. a., Freidenreich, S. M., Garner, S. T., Gudgel, R. G., Gordon, C. T., Held, I. M., Hemler, R. S., Horowitz, L. W., Klein, S. a., Knutson, T. R., Kushner, P. J., Langenhost, A. R., Lau, N. C., Liang, Z., Malyshev, S. L., Milly, P. C. D., Nath, M. J., Ploshay, J. J., Ramaswamy, V., Schwarzkopf, M. D., Shevliakova, E., Sirutis, J. J., Soden, B. J., Stern, W. F., Thompson, L. a., Wilson, R. J., Wittenberg, A. T., and Wyman, B. L. (2004). The new GFDL global atmosphere and land model AM2-LM2: Evaluation with prescribed SST simulations. *Journal of Climate*, 17(24):4641–4673.
- Bonan, G. B. (1996). A Land Surface Model (LSM Version 1.0) For Ecological , Hydrological , and Atmospheric Studies : Technical Description and User’s Guide.
- Bonan, G. B. (2002). *Ecological climatology: concepts and applications*. Cambridge University Press, 1 edition.
- Dickinson, R. E., Henderson-Sellers, A., Kennedy, P. J., Dickinson, E., Henderson-Sellers, A., and Kennedy, J. (1993). Biosphere-atmosphere Transfer Scheme (BATS) Version 1e as Coupled to the NCAR Community Climate Model. *NCAR Tech. Rep. NCAR/TN-3871STR*, 72, (August):77.
- Hurrell, J. W., Holland, M. M., Gent, P. R., Ghan, S., Kay, J. E., Kushner, P. J., Lamarque, J. F., Large, W. G., Lawrence, D., Lindsay, K., Lipscomb, W. H., Long, M. C., Mahowald, N., Marsh, D. R., Neale, R. B., Rasch, P., Vavrus, S., Vertenstein, M., Bader, D., Collins, W. D., Hack,

- J. J., Kiehl, J., and Marshall, S. (2013). The community earth system model: A framework for collaborative research. *Bulletin of the American Meteorological Society*, 94(9):1339–1360.
- Lawrence, D., Fisher, R., Koven, C., Oleson, K., Swenson, S., Vertenstein, M., Ben, Andre, B., Bonan, G., Ghimire, B., van Kampenhout, L., Kennedy, D., Kluzek, E., Knox, R., Lawrence, P., Li, F., Li, H., Lombardozzi, D., Lu, Y., Perket, J., Riley, W., Sacks, W., Shi, M., Wieder, W., and Xu, C. (2018). Technical Description of version 5.0 of the Community Land Model (CLM). Technical report, National Center for Atmospheric Research, Boulder, Colorado.
- Manabe, S. (1969). Climate and the Ocean Circulation 1. *Monthly Weather Review*, 97(11):739–774.
- Milly, P. C. D. and Shmakin, a. B. (2002a). Global Modeling of Land Water and Energy Balances. Part I: The Land Dynamics (LaD) Model. *Journal of Hydrometeorology*, 3(3):283–299.
- Milly, P. C. D. and Shmakin, a. B. (2002b). Global Modeling of Land Water and Energy Balances. Part I: The Land Dynamics (LaD) Model. *Journal of Hydrometeorology*, 3(3):283–299.
- Monin, A. S. and Obukhov, A. M. (1954). Basic laws of turbulent mixing in the surface layer of the atmosphere. *Contrib. Geophys. Inst. Acad. Sci. USSR*, 24(151):163–187.
- Neale, R. B., Gettelman, A., Park, S., Chen, C.-C., Lauritzen, P. H., Williamson, D. L., Conley, A. J., Kinnison, D., Marsh, D., Smith, A. K., Vitt, F., Garcia, R., Lamarque, J.-F., Mills, M., Tilmes, S., Morrison, H., Cameron-smith, P., Collins, W. D., Iacono, M. J., Easter, R. C., Liu, X., Ghan, S. J., Rasch, P. J., Taylor, M. a., Gettelman, A., Lauritzen, P. H., Park, S., Williamson, D. L., Conley, A. J., Garcia, R., Kinnison, D., Lamarque, J.-F., and Others (2012). Description of the NCAR community atmosphere model (CAM 5.0). *NCAR Tech. Note NCAR/TN-486+STR*.
- Paterson, W. S. B. (1994). *The physics of glaciers*. Pergamon, Oxford, OX, England; Tarrytown, N.Y., U.S.A., 3 edition.